Advanced Energy Conversion Materials
http://ojs.wiserpub.com/index.php/AECM/

UNIVERSAL WISER PUBLISHER

Review

Insight on Electronic and Thermal Behaviors of Conductive MXene-$Ti_3C_2T_x$-Based Polymeric Hybrid Material and Their Capacitive Energy Storage Applications: A Review

Anthony Chidi Ezika[1*], Christopher Chiedozie Obi[2], Henry Chukwuka Oyeoka[2], Uzoma Ebenezer Enwerem[2], Ugwu Shadrack Chukwuemeka[2], Ibenta Martin Emeka[2]

[1]Institute of NanoEngineering Research (INER), Department of Chemical, Metallurgical and Materials Engineering, Faculty of Engineering and The Built Environment, Tshwane University of Technology, Pretoria, South Africa
[2]Department of Polymer and Textile Engineering, Faculty of Engineering, Nnamdi Azikiwe University, Awka, Anambra State, Nigeria
Email: tonero2017@gmail.com

Received: 4 March 2024; **Revised:** 15 May 2024; **Accepted:** 16 May 2024

Graphical Abstract

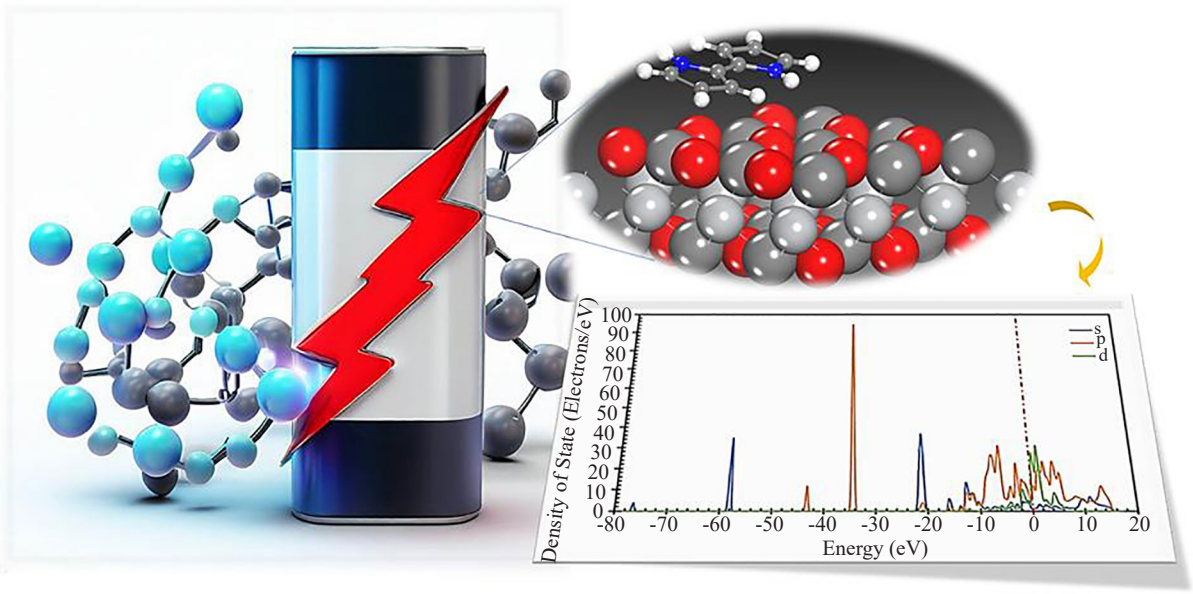

Abstract: The increasing research focus on two-dimensional carbides known as MXenes has garnered significant attention due to their effective capacitive properties, leading to their application in energy storage devices. Recently, the emerging technique of incorporating MXene into polymer matrices to form hybrid nanoclusters has significantly

DOI: https://doi.org/10.37256/aecm.5220244550

contributed to modern nanoarchitectonics. However, there is no available review that elaborately discusses the thermal and electrical behaviors of these hybrid nanoclusters. This paper provides detailed insights into the thermal and electrical properties of conductive MXene-$Ti_3C_2T_x$-based polymeric hybrid nanoclusters. Further elucidation is given to their applications in energy storage devices, with a special interest in MXene-polypyrrole, MXene-polyaniline, and MXene-poly (3, 4 ethylenedioxythiopene) polystyrene sulfonate nanoclusters. Additionally, to address the challenges associated with electron transport within the atoms of the nanoclusters, we concluded by offering suggestions on a potential approach to alleviate these challenges and enhance their electrical performance for future applications.

***Keywords*:** thermal properties, electrical properties, MXene-polymeric hybrids, nanoclusters, energy storage applications

1. Introduction

The attempt to solve the energy crisis has led to research on energy storage devices with attention given to the use of 2-D materials such as borophene, graphene nanosheets, exfoliated graphene, phosphorene, and silicene [1]. This is due to their low weight, high electron mobility, chemical stability, thermal and electrical conductivity, and flexibility [2]. Recently, a 2-D material known as MXene-$Ti_3C_2T_x$ was produced by the exfoliation of Ti_3AlC_2 [3]. Generally, MXene is fabricated from the transition metallic nitrides, carbides, and carbonitrides known as MAX-phases with the formula $M_{n+1}AX_n$, (where n = 1, 2, 3 or 4; X represents carbon, nitride, or carbon nitride; M represents a transition metal, and A represents the periodic group 13 or 14 elements). MXene is synthesized through the etching of A elements [3] with surface terminations Tx, to give the general formula $M_{n+1}AX_nT_x$, (where T represents the functional group (-Cl, -O, -F, or -OH), x is the small part of the functional group). For energy storage applications, MXene presents so many advantages over other energy storage materials [4]. The surface chemistry of MXene, significantly contributes to its oxidative property, allowing the formation of composites with other capacitive materials. Like the other 2-D materials, MXene can be loaded into several materials to achieve the desired properties for targeted applications [5]. Among these materials are polymers that form MXene-polymer composites [5].

Generally, polymers are studied to have high electrical and thermal resistance, hence they are perceived to be insulators [6-10]. The inclusion of conductive nanofillers such as MXene-$Ti_3C_2T_x$ into the polymer matrix has a significant change in the thermal and electrical conductivity of the resulting MXene-polymer nanocomposites (PNC) [11-15]. Several properties of MXene have been reported to improve by the addition of polymers. Such properties involve flame retardancy, stretchability, toughness, thermal stability, electron mobility, and chemical resistance [16-19]. Nowadays, MXene-polymer composites have been utilized as an engineering material for many applications ranging from biomedical, energy storage, electronic, and electromagnetic shielding, to photovoltaic applications [5, 17, 20-22].

On the other hand, several polymers have an inherent conductive nature, hence they are called conductive polymers [23-27]. Among these polymers are conductive polypyrrole (PPy), polyaniline (PANI), and poly (3, 4 ethylene dioxythiophene) polystyrene sulfonate (PEDOT:PSS) which have alternating double and single bonds at the backbone chain (Figure 1) with their overlapping p-orbitals forming a system of delocalized π-electron, which induces electron transfer. Hence, they are also referred to as conjugate polymers [28]. Conductive polymers, intrinsically, exhibit the ability to conduct electricity. They are positioned beyond insulators while showcasing metallic behavior, otherwise, classified as synthetic metals. This results in their useful inherent electronic properties, and their applications in both energy storage and thermoelectric devices [29-39].

The hybrids of MXene and conductive polymers have showcased innumerable advantages in the design of electrodes for energy storage devices (ESDs) [40, 41], hence, the study of their thermal and electrical behavior is paramount as regards energy storage. ESDs when in use, ranging from supercapacitors to batteries, generally, are subjected to temperatures between -40 °C to 60 °C [42, 43]. At this temperature range, the electrode is expected to deliver optimum performance with suitable thermal stability and thermal conductivity, without any degradation. Generally, the incorporation of nanofillers (MXene) into a polymer matrix will cause an obvious enhancement in properties which of course includes thermal stability/conductivity [44]. MXenes have a high surface area, hence a very large interfacial area and bonding sites, when adequately incorporated into a polymer matrix. MXene tends to alter the properties of the polymer in those interfacial areas, and as such, a larger area of modified properties will be achieved even at lower MXene content. This will result in a pronounced change in the macroscopic thermal property of the

MXene-polymer nanocluster [45]. The mechanism of thermal stability of MXene nanoclusters can be likened to that of graphite with a similar structure of layered nano thickness of approximately 10 nm. Following the highly anisometric structure of the fundamental particles of layered MXene, and its inherent thermal resistance, heat, and gas diffusion are likely to be prevented by forming physical barriers, thereby delaying the mass loss of polymer during degradation [45]. Moreover, the surface functional groups that exist on MXene nanosheets, which form strong bonds with the polymer, suggest enhanced thermal properties in MXene-based polymer nanocomposites [46].

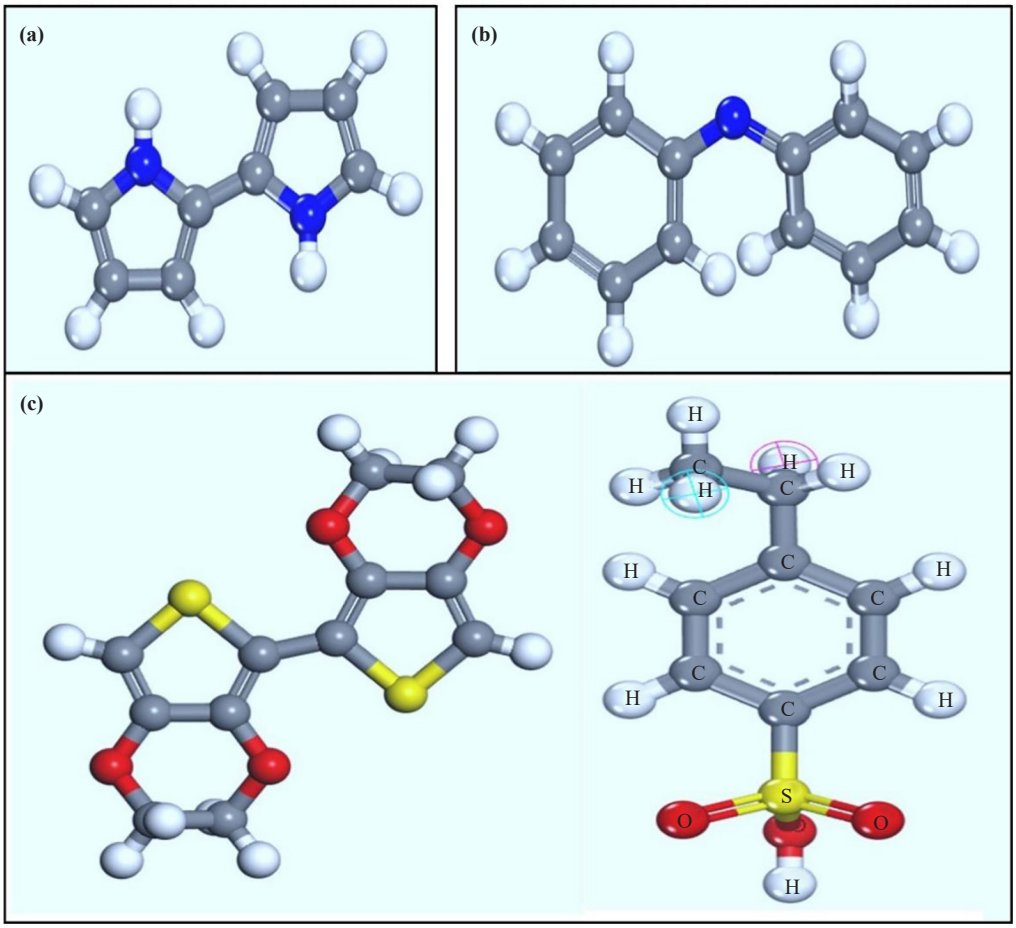

Figure 1. The 3D chain structure of the dimer of (a) PPy; (b) PANI; (c) PEDOT:PSS

The contribution of polymer to the thermal stability of MXene-polymeric nanoclusters has been reported [47]. In the thermogravimetric analysis (TGA) of MXene ($Ti_3C_2T_x$) and MXene-Poly vinyl alcohol (MXene-PVA) in both nitrogen and oxygen environments, pure MXene decomposed at the temperature of 785 °C, and MXene-PVA composite decomposed at the temperature of 823 °C, both in a nitrogen atmosphere. This implies that the MXene-PVA has better thermal stability than pure MXene in a nitrogen atmosphere. Again, in an oxygen atmosphere, pure MXene decomposed at the temperature of 729 °C, while MXene-PVA decomposed at the temperature of 811 °C. This suggests that the addition of polymer to MXene enhanced the thermal stability of MXene in both nitrogen and oxygen atmospheres. Hence, polymer encapsulation protects MXene from environmental oxidation in the presence of atmospheric air [48]. Also, the degree of dispersion of MXene layered sheets inside the polymer matrix contributes to the effective bonding of the composite, as this will create evenly distributed bonding sites, thereby allowing MXene nanosheets to protect more polymer particles against thermal degradation, hence the overall electrode is made thermally stable. It has been reported that the degree of nanofiller dispersion and its percentage loading affect the thermal properties of the polymer

nanocomposites [49, 50]. Dipika et al. reported the effect of MXene and its percentage loading on the weight loss of MXene polymeric nanocomposites for flexible energy storage materials [51]. The overall thermal behavior of MXene-based conducting polymer hybrid nanoclusters can also be attributed to the percentage loading and the degree of dispersion of MXene in the conducting polymers.

On the other hand, the electrical performance of the electrode also contributes to the overall performance of the supercapacitors and batteries. The electron transport ability of an electrode strongly depends on the material molecules of the electrode and its chemical/electrochemical environment. This is most effective when the probability of electron transmission through the molecules of the electrode material is near 100% [52]. Again, the molecular length, the connection means, the presence of alternating single and double bonds, and the inclusions of possible carbon clusters (carbon derivatives) within the molecular network of the electrode material have a significant effect on the electrical conductivity of the electrode [52]. This electron transport behavior in nanoclusters is significantly important in the design of electrodes for device applications, most especially in energy storage applications, where the balance in ions storage and electron transport must be maintained for efficient electrochemical performance. Figure 2 shows the various electron transport through different molecular chains. Benzene depicts the simplest type of electron transport in a single molecule with a large energy gap between the conduction and valence bands, and as such, has lesser conductance (see Figure 2a). The electron transport in graphene with little or no energy gaps, following the clustering of the benzene ring, is without restriction. Hence, a high conductance is seen in graphene molecules. The nano-clustering of MXene and conducting polymers utilizes the idea of bridging the gap between the conduction and valence bands, with the polymer molecules creating a pathway for efficient electron transport as revealed using the density functional theory (DFT). Figure 3 shows the intercalation/clustering of PPy in between the MXene layers, creating a pathway for efficient electron transport.

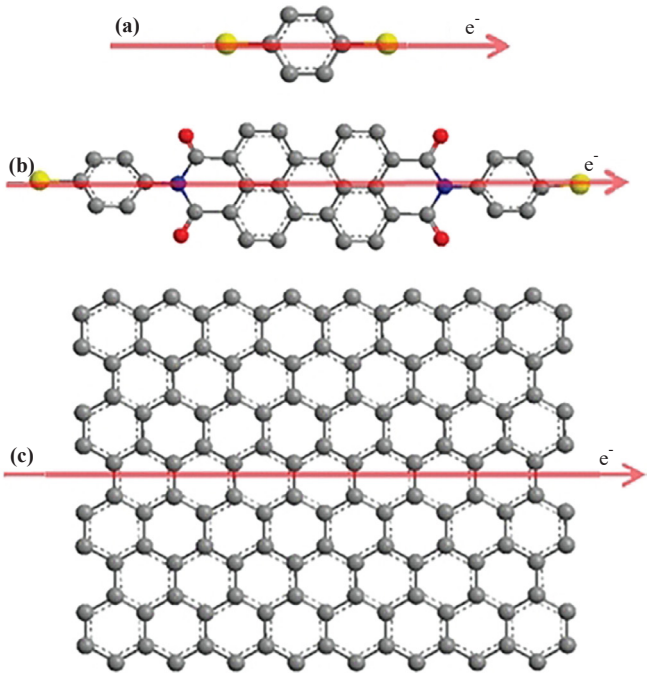

Figure 2. Electron transport in various molecular chains (a) electron transport in a single benzene molecule; (b) electron transport in a compound with fewer molecular chains; (c) electron transport in graphene. Reproduced with permission from Ref. [52]

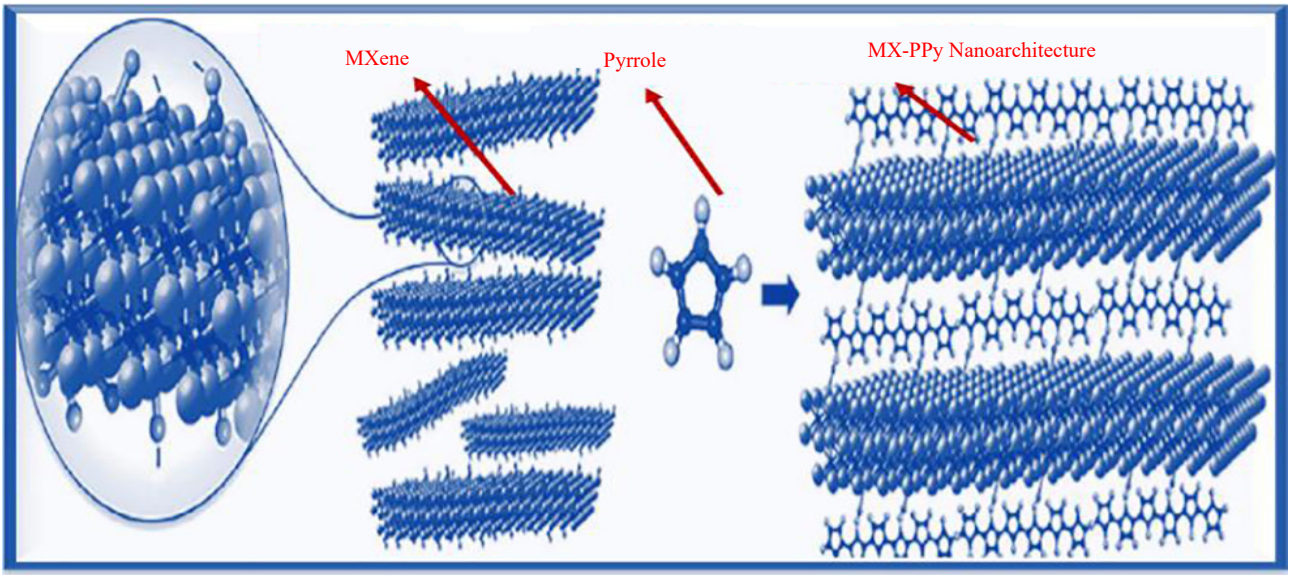

Figure 3. The intercalation of PPy in-between MXene nanolayers to form nanoclusters for efficient electron transport. Reproduced with permission from Taylor and Francis [40]

The study of the electron transport and photon emission of MXene-polymeric hybrid nanoclusters, not only answers the basic questions about the electrical conductivity and thermal conductivity of the conductive nanoclusters but also contributes to the ongoing pursuit of molecular-scale electronic devices. This paper focuses on elucidating the thermal and electrical behaviors of conductive MXene-$Ti_3C_2T_x$-based polymeric hybrid nanoclusters. It discusses their potential applications in capacitive energy storage, particularly about MXene-conjugate polymers, which include MXene-PPy, MXene-PANI, and MXene-PEDOT:PSS. Also, insights are provided on the approach to remedy the insufficient charge carriers, which is a challenge for the use of MXene-based polymeric hybrid nanoclusters for energy storage applications.

2. MXene as a capacitive material for energy storage applications

MXenes are a wide family of 2-D materials (Figure 4b), which can be selectively etched from several atomic layers of MAX-phases (Figure 4a). These ternary transitional metals of carbides/nitrides are composed of layers of group 13 and 14 elements "A", closely packed atoms of "M", and X atoms which occupy the octahedral sites. So far, more than 70 different MAX-phases have been discovered [53], which includes the obvious pure MAX-phases. Following the difference in the bonding strength between M-X and M-A, the elemental layer "A" can be etched selectively with proper temperature and etchant to give a 2-D layered structure of MXene. Several etchants have been employed to fabricate MXene from MAX phases while preserving its 2D structure.

The obvious use of MXene as a capacitive material for energy storage applications is renowned [54-58]. This is due to its likely properties with graphene which include the interlayer spacing of its molecules, which is majorly explored for energy storage in the form of ions/charges in an electrochemical setup for later discharge, resulting in the release of the energy in the form of electron movement [59, 60]. The clustering architecture of a single MXene sheet (Ti_3C_2) as shown in Figure 4a is extracted from its metallic carbide lattice. This MXene single sheet is readily oxidized which contributes to its thermal instability when compared with the metallic carbide MAX-phase [61-64].

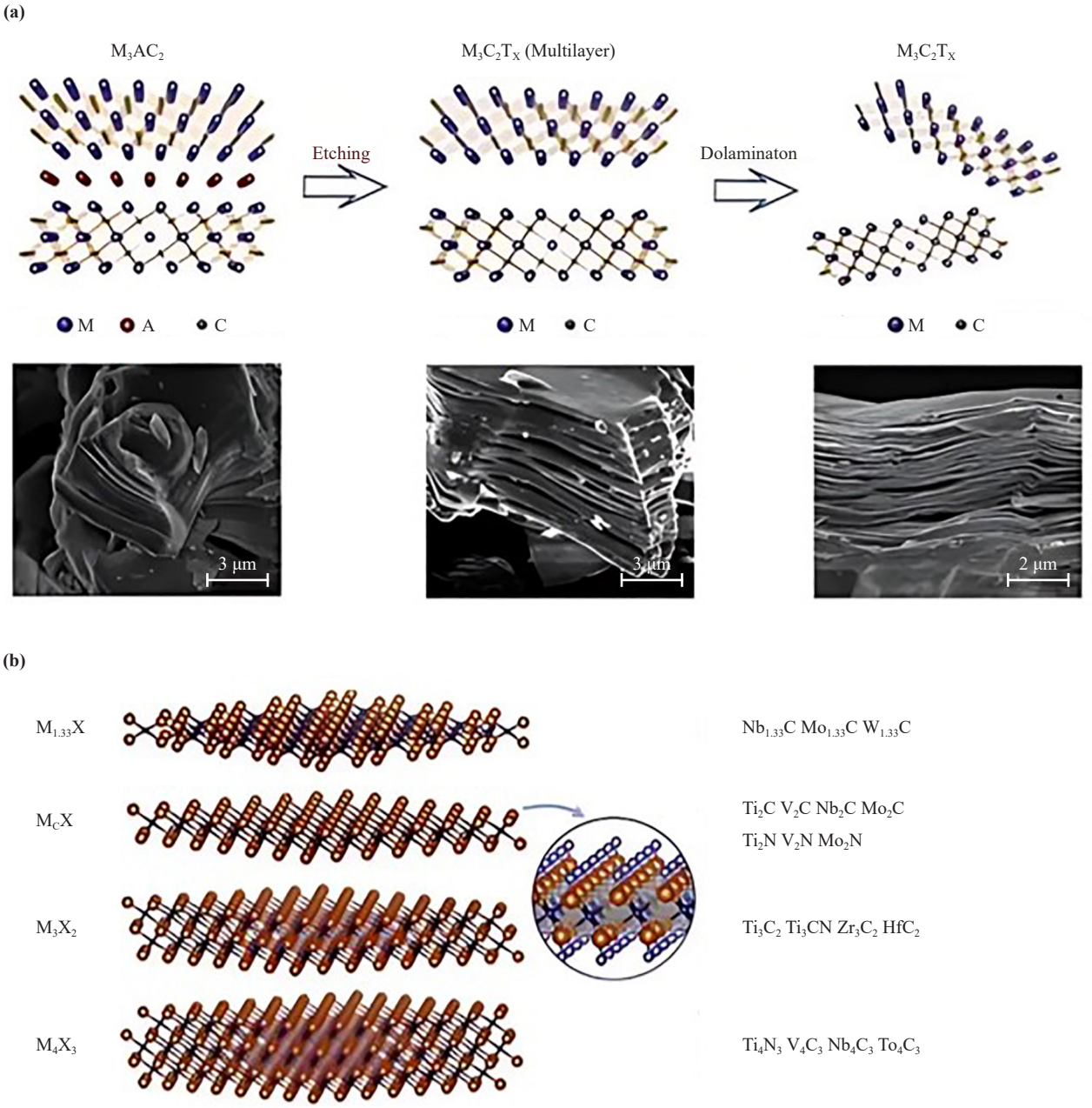

Figure 4. (a) Schematic illustration, and the SEM images of the fabrication process of MXene from the MAX phases. b) Different MXenes synthesized experimentally so far. Reproduced with permission from Elsevier [65]

2.1 *Synthesis of MXene ($Ti_3C_2T_x$)*

The top-down etching method remains the most common technique for synthesizing MXene, by etching "A" from the MAX phase (Ti_3AlC_2), where A is aluminum; M represents the transition metals, which in this case is Titanium; whereas X is the carbide group [66, 67]. Generally, the bond that exists in the MAX phases is both metallic and covalent [68], which requires an etchant to weaken the bond and allow the removal of aluminum from the MAX phase [69]. Till now, research has been ongoing in the quest to discover the best etchant for the complete removal of aluminum without the leaching of M or X, which will result in achieving a higher mass deposit of MXene. Several etchants have been employed in the etching of aluminum from MAX phases, ranging from acidic medium (HF, LiF, HCl) [70-75] to

alkaline medium (NH_3OH) [76-78]. The synthetic metal carbide is similar to graphene which belongs to the class of 2D materials, it is commonly known as MXene [79]. Following the initial awareness of MXene in 2011, this material was originally fabricated through the HF etching of its precursor, the MAX phase as shown in Figure 4a.

The top-down pathway involves the etching and delamination of the MXene into nanosheets [80, 81]. The HF etching of Aluminum leaves the MXene surface with terminations of -O, -OH, and -F [82-84], this initiates intercalation of the cations which assists in MXene delamination into mono or bi-layered MXene-nano sheets.

Additionally, MXenes synthesized via HF are characterized by tiny hole voids, this allows Titanium ions to react with air by oxidation which results in the formation of Titanium oxide [85-87]. When compared to the Li-HCL etching route, $Ti_3AlC_2 + 3H^+ + 3F^- = AlF_3 + 3/2H_2 + Ti_3C_2$, known as the clay approach, following the clay-prone formation of LiF-HCl-$Ti_3C_2T_x$. LiF-HCl-$Ti_3C_2T_x$ is hydrophilic due to the presence of OH molecules. As the etching proceeds, there is twice an increase in volume, due to the wetting of the intercalated lithium [88].

Furthermore, the etching detection follows LiF and HCL constituents, as intercalation of Li-ion characterizes the former, while the degree of etching showcases the latter. Again, when compared with the HF-etching route, the Li-HCl etching route is more yielding, as the etching system shows high interface and surface quality and enhanced mechanical stability. This was observed from the dimensions of the MXene sheets, which are larger without sonication.

Again, the use of dilute HCl through electrochemical etching was employed to remove aluminum from its MAX-phase (Ti_3AlC_2) to obtain a porous and layered sheet of MXene. The surface terminations on these MXenes were found to be Cl, -O, -OH groups [75]. In another research, Zhang et al. [88] utilized a binary aqueous salt comprising 1M ammonium chloride and 0.2 M tetramethylammonium hydroxide for the removal of aluminum from Ti_3AlC_2 through an electrochemical technique. This route provides MXene with a large lateral dimension and a high yield of bilayer or mono-layer MXene nanosheet. Also, an organic base etchant (TMAOH) was utilized to remove aluminum from the multi-layer of Ti_3AlC_2 [89]. This method involves the hydrolysis of aluminum by TMAOH to form Ti_3C_2- MXene with intercalated TMA^+.

Nevertheless, the geometry of the synthesized MXene is affected by the etching temperature, etching duration, and etching route [67, 90]. The surface chemistry, induced by the etching process, which involves the terminations of -OH, -F, and so on, inhibits the further etching of aluminum. Hence, increasing the etching temperature increases the degree and rate of etching [91]. The performance of MXene for energy storage can be optimized and harnessed by the introduction of a porous structure [92]. Due to the force of attraction that exists between MXene interlayers, MXene lacks the desired porosity for energy storage applications. Bu et al. [93] suggest that adding other materials into MXene, and freeze-drying MXene after exfoliating, can result in porous MXene for capacitive energy storage applications.

2.2 *Capacitive properties of conductive MXene for energy storage applications*

Density functional theory (DFT)/molecular dynamics (MD) models revealed that the atomic composition of MXene has 2-D geometry compared to that of graphene [94-96]. When compared to other carbon materials, MXene has high density as well as surface functional groups, as a result of metallic constituents present in its chain [83, 97]. The inherently high density of MXene, when compared with other carbon-oriented substrates, has resulted in its high volumetric capacitance [98]. Also, MXene shows metallic conductivity and hydrophilicity, this assists in fast electron transport in addition to the wetting of the electrolyte.

The modifiable surface functional groups that exist on MXene, result in its exceptional attributes. For instance, the -O entity, on the MXene surface, provides bonding sites for redox reactions [99, 100]. Moreover, the negative functional groups on the MXene surface contribute to the negative nature of MXene surface charges, and bonding between MXene and water via hydrogen bonding, hence the even dispersion nature of MXene in a solvent [99]. Due to the MXene architecture and geometry, it addresses the defects associated with electrodes made from other carbon-oriented materials for capacitive energy storage applications [101] as shown in Figure 5.

MXene shows a range of capacitive behaviors, depending on the architecture, functional groups, and the dimensions of the electrolyte cations [59, 80, 102]. Inherently, the MXene surface contains termination functional groups of -OH, -F, and -O. During the movement of electrolyte cations, around and within the layers of MXene, an electrostatic attraction occurs between the two unlike charges [103, 104]. This will cause the minute electrolyte cations to penetrate and diffuse into the MXene layers which will result in the altering of the electrode molecular structure, and as such, a pseudo-capacitance is said to have occurred. However, during the penetration of the electrolyte cations,

the bigger cations are restricted from diffusion due to the electrostatic repulsion which maintains high cycle stability through electrochemical adsorption [105]. Finally, MXenes are used as fillers to modify and improve the capacitance, thermal, and electrical properties of various materials including polymers [17, 41, 106-113].

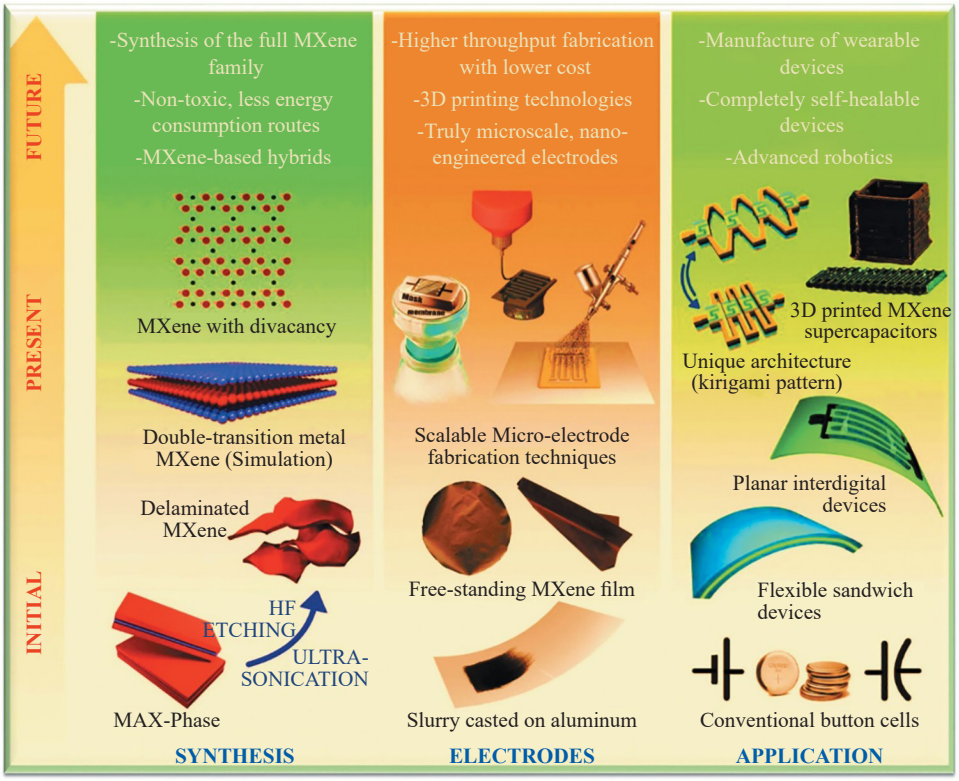

Figure 5. (Left) synthesis of MXene through HF MAX etching, under sonication to form a delaminated single nanosheet, presently a 2-D double transition metal MXene realized through simulation, and in the future, less energy consumption routes for MXene and MXene-hybrids will be achieved. (Middle) evolution of the application of MXene in electrode design, from slurry cast on aluminum to free-standing MXene film, scalable micro-electrodes, and in the future a higher throughput fabrication with lower cost via 3-D printing. (Right) capacitive MXene-designed batteries and supercapacitors to wearable energy storage devices. Reproduced with permission from Taylor and Francis [4, 40]

3. Fabrication techniques of conductive MXene-based polymeric hybrid nano-clusters

To achieve improved MXene-polymeric nanocluster properties, even and effective dispersion of exfoliated MXene layers into the polymer matrix is of utmost importance. Even so, it is paramount to demonstrate that reinforcement with monolayers might not necessarily improve the mechanical properties, as revealed by using graphene-reinforced polymer hybrids [114]. There, it was shown that the hybrids' optimum modulus was achieved with a mono sheet of tri-layered graphene of 1 nm thickness. Therefore, considering the numerous advantages associated with scalability, MXene with multi-layer may be a practicable option for reinforcing polymeric nanoclusters, this will necessitate the need for MXene delamination.

To achieve both efficient dispersion and exfoliation of MXene, the method through which the MXene nanosheets are introduced into the polymer matrices to form nanoclusters affects their clustering as well as their properties. Mainly, three nanocluster processing techniques are widespread and accepted, namely, in situ polymerization, solvent blending, and melt blending.

3.1 *In situ polymerization approach*

A significant effective approach for fabricating nanoclusters involves the polymerization of monomer in the presence of inclusions/fillers, hence, an in-situ polymerization [115-117] (Figure 6). This technique provides the formation of polymeric chains nearer to the inclusion surfaces. Intercalation of monomers in-between the layered materials such as MXene, through polymerization, results in spacing and exfoliation of MXene nanosheets.

Reports for in situ polymerizations of MXene polymeric hybrid nanoclusters [5, 19, 113, 118, 119] have shown that improved nanoclusters' properties can be attained through an in situ polymerization approach. This can be attributed to the proximity of the polymeric chain gradient to the entire surface area of the nanofillers. Where MXene is embedded in a material, maybe a resin, followed by the filling of the second material, this will prompt a polymerization reaction, as the unsaturated polymer will react with the surface-functionalized MXene to form nanoclusters. Alternatively, an aqueous medium can be utilized to facilitate an in-situ polymerization reaction, as shown by various polymers [120-125].

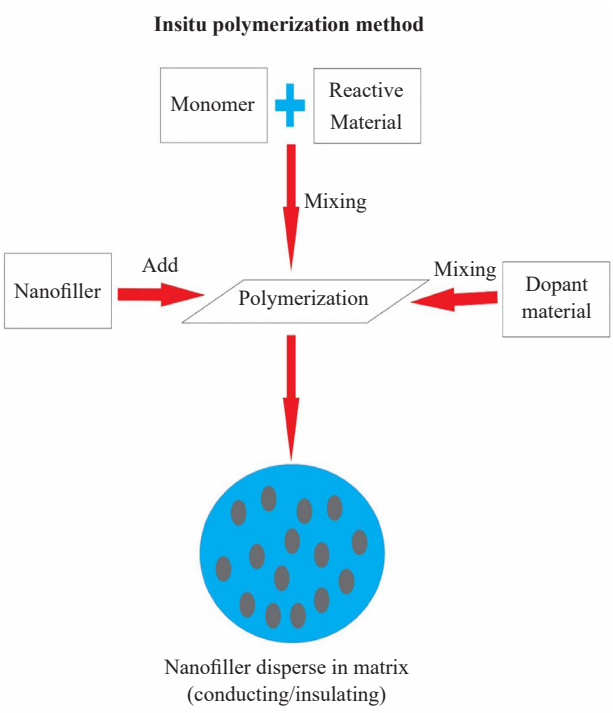

Figure 6. In situ polymerization approach of preparation for both insulating and conductive polymeric nanoclusters [126]

3.2 *Solvent blending approach*

Solvent blending, otherwise called solution mixing portrays the most common pathway for MX-polymeric nanoclusters preparation. The approach involves the usage of a solvent medium to disperse and include the MXene nanosheets into, and unto the polymer matrix through colloidal agitation [29] (Figure 7). However, the choice of solvent is of interest in the solvent blending technique, as it is limited to polar solvents. This is a result of MXene's inherent solubility in polar solvents, hence, its compatibility with solvents of similar solubility parameters [29]. However, various surface treatments can cause MXene solubility in non-polar solvent entities. On the other hand, polymer matrices are also limited to several solvents. To achieve an effective solvent blending of MXene and polymers, the colloidal solution system may be thermodynamically altered, with the solvent compatible with both MXene as well as the polymer [28].

Oftentimes, after blending, MXene-nanoclusters are realized from the solution through evaporation, vacuum filtration, or precipitation to achieve a zero-solvent state. Various MXene-nanoclusters have been prepared to utilize

water-compatible polymer matrices such as cellulose nanofibrils, polyallylamine hydrochloric, PA, PAA, polydopamine, PEO, PEDOT:PSS, polyether polyamide block co-polymer, and PVA [29].

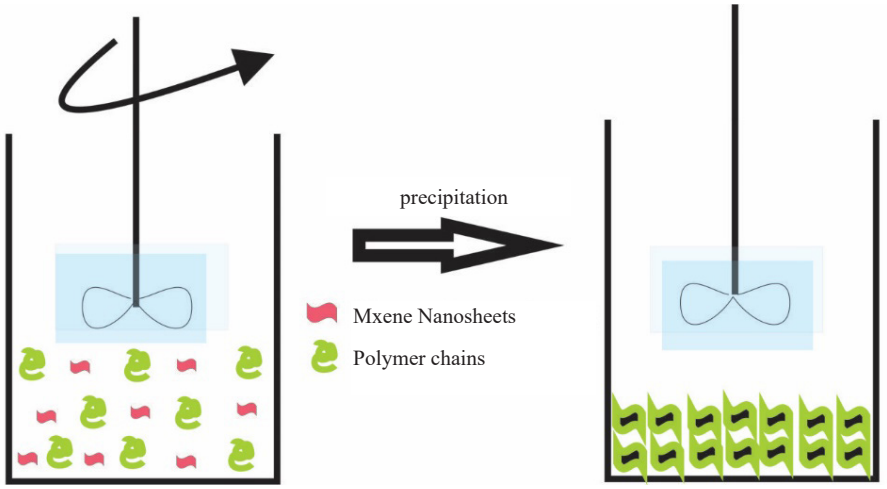

Figure 7. Solution blending of Polymers and MXene nanosheets to form nanoclusters

3.3 *Melt blending process*

In melt-blending, the incorporation of MXene into the polymer matrix is achieved above the polymer melting point. This is to allow the movement of the polymer chain to welcome the MXene nanosheets and possible grafting into the polymeric chain [63]. Melt blending involves processing techniques such as injection molding, extrusion, and sintering that can be employed to achieve MXene nanosheets even dispersion within and unto polymer matrices. These processes are mainly utilized for the blending of large-scale nanoclusters to achieve uniform clustering. However, most thermosetting polymers are not blended through this approach which is most likely employed for thermoplastic polymers. Also, high-temperature blending may cause oxidation of MXene as well as polymer chain deterioration. Notably, when compared with other 2-D materials relative to this blending technique, MXene has the advantage of high bulk density, which facilitates material transport through the hopper during the production process. Melt blending has been employed in the preparation of most MXene-thermoplastic-polymeric nanoclusters including MXene-PS, MXene-nylon 6, MXene-polyurethane, and MXene-phthalonitrile [28-29]. Surface treatment of MXene is often carried out to achieve good adhesion with the polymer matrix for optimum nanocluster properties, especially thermal properties.

3.4 *Electrodeposition technique*

The electrodeposition technique, conventionally called electroplating, is a vital technique employed for the fabrication of nano-clustered materials, which allows control over the properties, composition, and structure. The technique helps in the preparation of special materials with desirable enhanced properties which cannot be achieved through other techniques. The flexible low cost of the technology has given its use in the preparation of three- and two-dimensional materials which include films. The electrodeposition process is based on the principles of electrochemical occurrence related to the deposition or reduction of electroactive elements and compositional species on the cathode surface. This technique has been reported for the fabrication of MXene-polymeric nanocomposites, which involves the in-situ polymerization and deposition unto the desired material usually a glass electrode [19, 127, 128]. Hence, it is often employed for the coating of materials using polymer nanocomposites. However, controlling and designing of electrodeposition process involves many experimental factors for harnessed redox reaction during the process [129]. In the preparation of MXene-polymeric nanocomposites which involves conjugate polymers, over-oxidation of the conductive polymers affected by the presence of the MXene is probable [130-132]. This reduces the electrical

conductivity of the prepared nanocomposites as a result of the formation of the oxides [133].

4. Thermal properties of conductive MX-based polymeric hybrid nanoclusters

Thermal properties of polymer composite as illustrated by Zhang, Choi [134], [135], depend on the concentration, size, type, filler dispersion, and very crucially, the presence of a thermal barrier between polymer chains. MXene has good thermal stability as well as excellent thermal conductivity. MXene, when added to thermal insulators that are usually polymers, can transform them into conductive equivalents. In comparison to graphene-based nanoclusters, which have thermal conductivities of 0.14 to 0.41 W/(m·K) at a 2 wt% loading [136, 137]. MXene-based polymeric nanoclusters have shown better thermal properties of 0.5 W/(m·K) with lower filler loadings [138, 139]. To promote heat transfer kinetics, thermal conductivity necessitates strong connections between the inclusions and the polymer. When the concentration of MXene is high enough to create a network, its high inherent thermal conductivity greatly exceeds the inherent thermal resistivity of the polymeric matrix, resulting in uniform thermal conductivity, and increased thermal stability [140]. This section tends to analyze the thermal properties of conductive MXene-$Ti_3C_2T_x$-based polymeric hybrid nanoclusters.

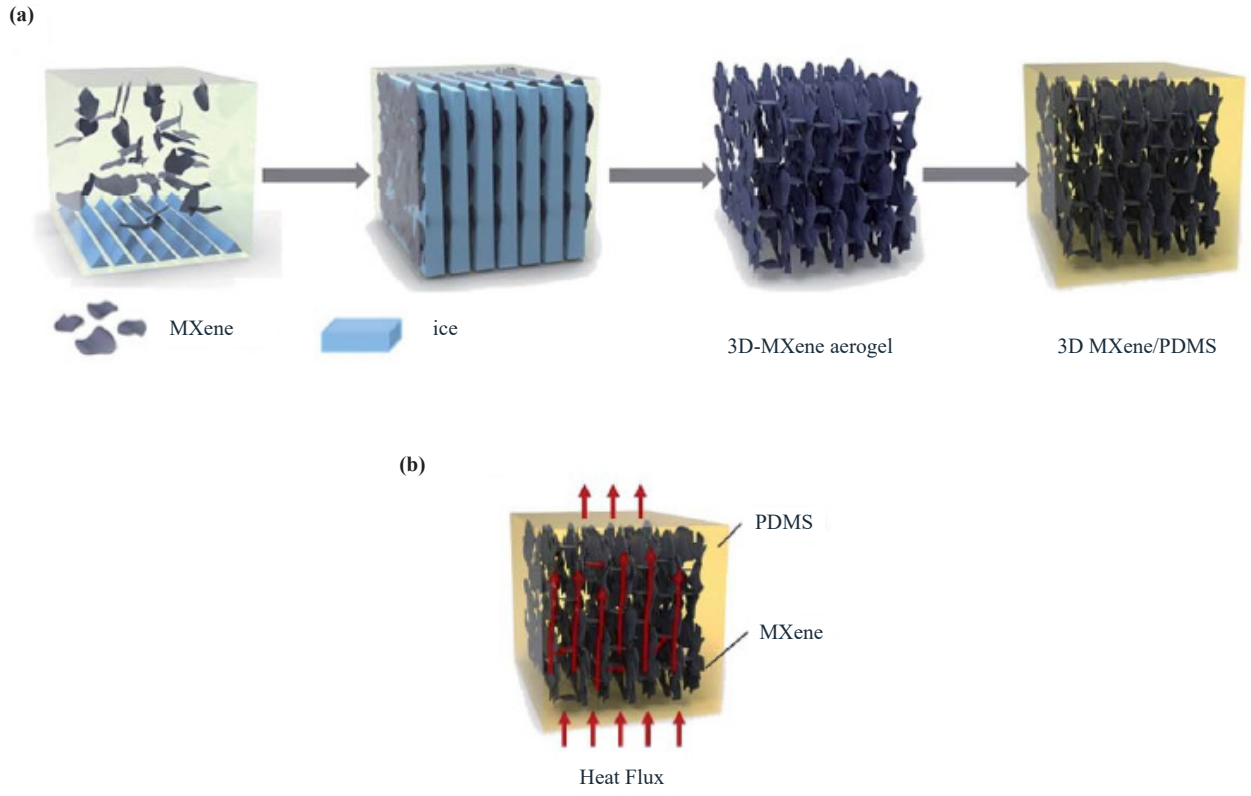

Figure 8. (a) the creation of a 3-dimensional MXene network through the freeze-drying approach, and inclusion in a PDMS matrix. (b) illustration of heat transfer pathways by MXene network in a PDMS matrix. Reproduced with permission from Ref. [11]

Based on theoretical calculations, the average MXenes' high thermal conductivities have been calculated to be 472, indicating its potential for usage in EMI shielding surfaces with excellent dissipation of heat [141]. However, regarding the macroscopic MXene-based nanoclusters for thermal conductive EMI shielding surfaces, fewer reports so far have been given. The easily-oxidized characteristics of MXene may contribute to its absence in thermal conductive EMI shielding film; taking example $Ti_3C_2T_x$ MXene, the numerous active functional groups (-OH, = O, and -F) on the

nanosheet surface are readily oxidized into TiO_2, especially in the high-temperature circumstances resulting in fast reduced electron and phonon transport efficiency on the MXene [142]. This will negatively impact thermal conductivity, making it unsuitable for use in EMI shielding devices [143].

Other researchers have looked into the thermal stability of MXene nanocomposite [144]. Creating a network between MXene sheets within the nanoclusters to build an MXene cluster is critical for developing an effective thermally conductive system. Percolation concentration is the concentration at which network creation occurs. Rather than randomly scattering MXene flakes, it is proposed to induce a 3-dimensional network of arranged MXene sheets within a polymer matrix to achieve low-concentration percolation as seen in Figure 8a.

As earlier said, the preparation of a one-directional, 3-dimensional porous MXene structure is probable by freeze-drying. As reported, the 3-D-oriented MXene structure inculcates excellent heat exchange pathways in a polymeric matrix (Figure 8b). The inclusion of just 0.7 wt% mono-layer Ti_3C_2 into the matrix of PDMS, a non-thermal conductive polymer, enhanced the thermal conductivity of the nanocluster by 220% and its thermal stability by 14 in arithmetic order of increase [145].

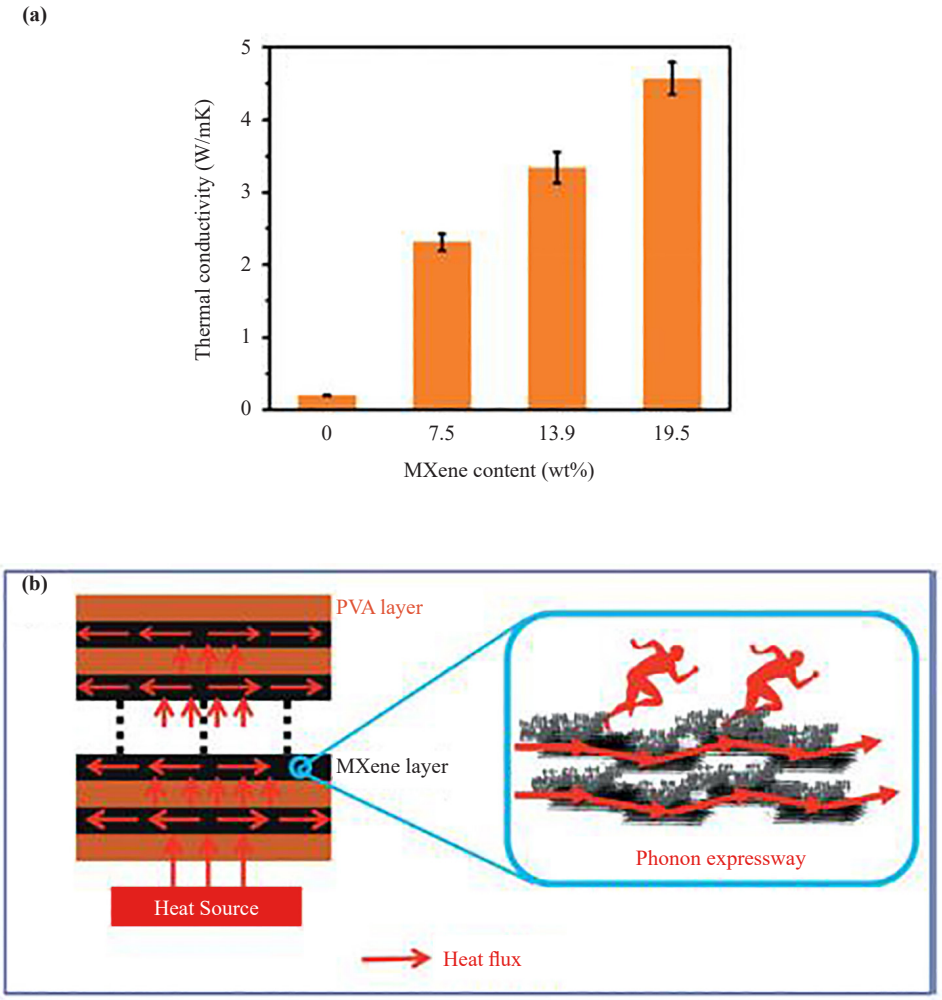

Figure 9. (a) plot of thermal conductivities of different MXene/PVA nanoclusters and pristine PVA; and (b) illustration of the thermal conductive pathways of MXene/PVA nanocluster. Reproduced with permission from Ref. [146]

Thermal conductivity and thermal conductivity mechanisms are shown in Figure 9. Relative to neat PVA, thermal conductivity was increased by 1,570%. The MXene forms a constant thermal conductive network throughout the matrix.

The heat flux was proficiently dissipated through the uninterrupted MXene layers [146].

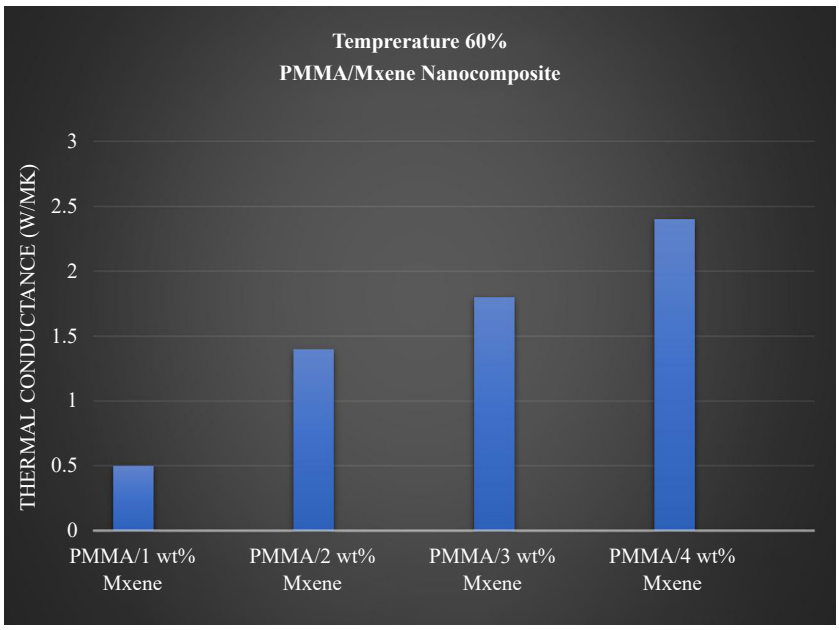

Figure 10. The effect of concentration of MXene on the thermal conductance of PMMA [148]

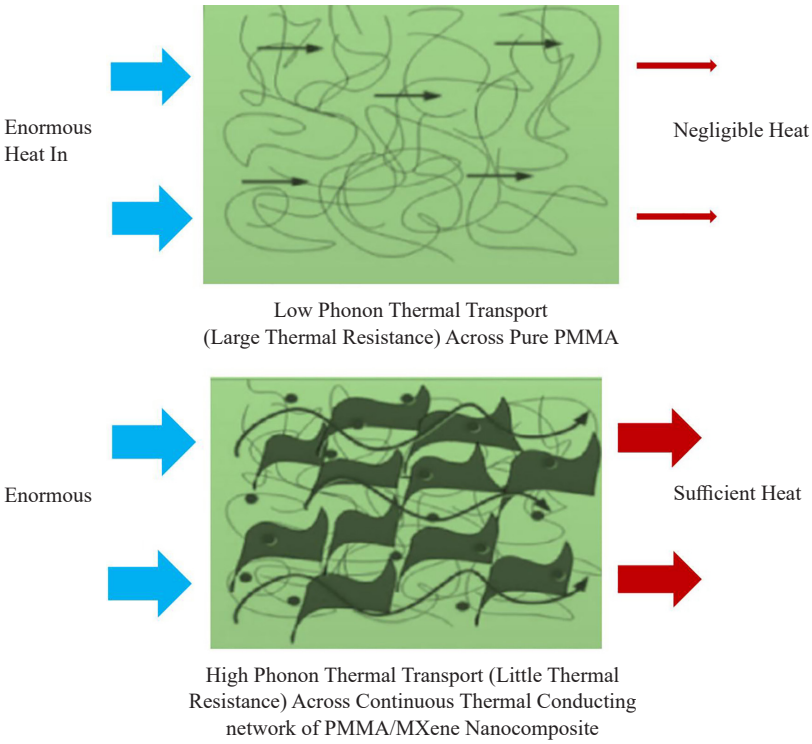

Figure 11. Illustration of thermal conductance of pure PMMA, and a composite of PMMA respectively [148]

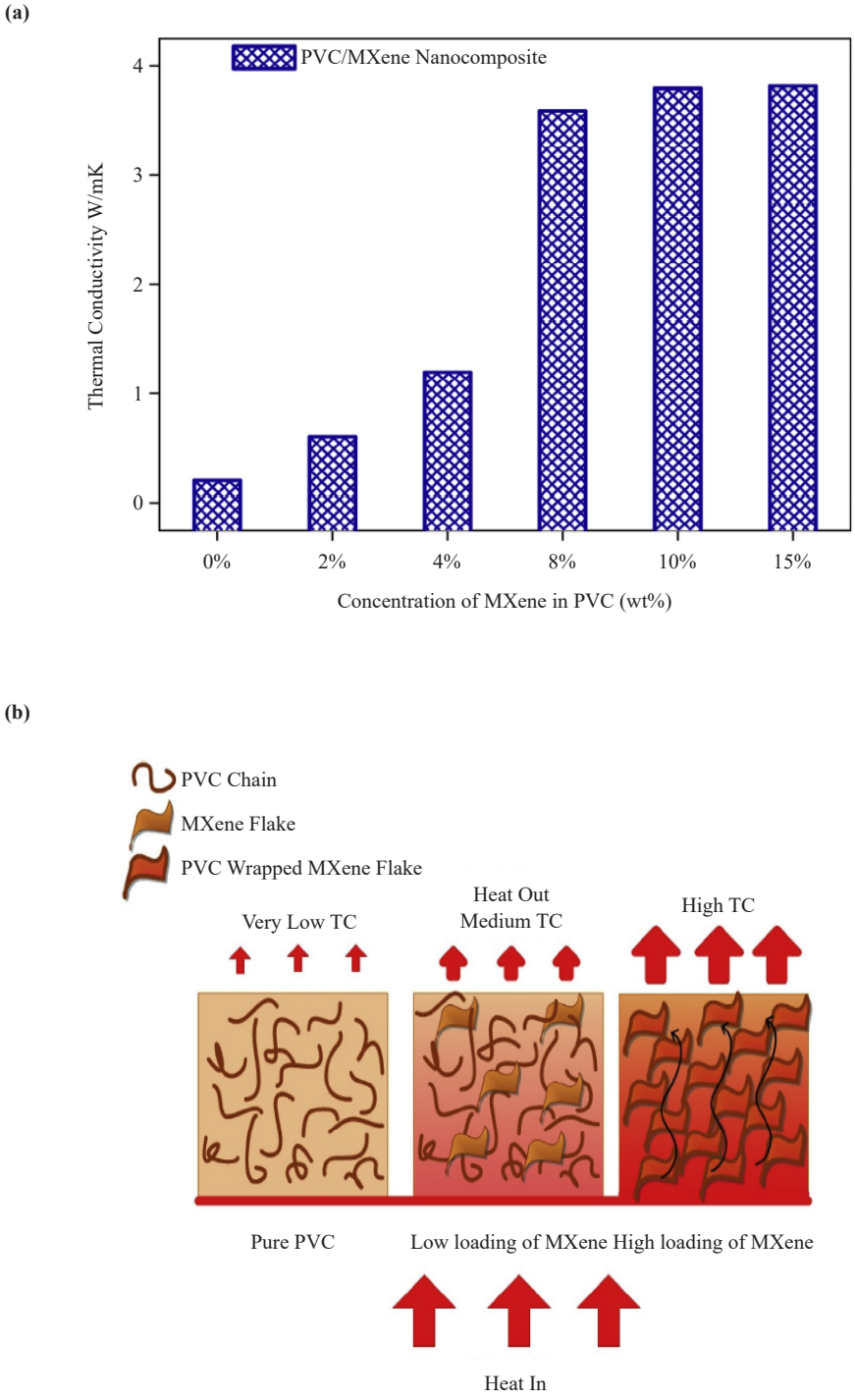

Figure 12. (a) Thermal conductivities of PVC/MXene nanoclusters Vs MXene loading, (b) diagram showing the thermal conductive network of PVC/MXene nanocluster. Reproduced with permission from Ref. [153]

The creation of a heat conduction network is one key mechanism responsible for the considerable improvement in the thermal conductance of PPMA. Because PMMA is an amorphous polymer with voids/spaces in its structure, increasing MXene content improves thermal conductivity by generating a heat conduction network [147]. However, the concentration of MXene significantly affects the conductivity of the polymer composite [134, 135]. MXene-

based nanocluster hybrid of PMMA/MXene was analyzed by Ul Haq, and Murtaza [148] using the common hot plate technique. A heat exchange contact that exists between the polymeric chain of PMMA is formed at a certain limit called the percolation threshold, here there's a high bridging ratio of MXene-MXene and the polymer chain [149]. Another reason for improved conductance according to Ul Haq, and Murtaza [148], is the distribution and compatibility of MXene within the polymer matrix. This results in strong surface and interfacial bonding of MXene sheets, which facilitates the transfer of heat by PMMA from one interface to another within the composite [150, 151]. Figure 10 shows the increasing heat transfer in the PMMA lactic structure due to the improving concentration of MXene. Another reason is the phonon scattering nature of MXene nanosheet which is due to the inherent high thermal conductivity, even distribution of MXene in the matrix, and high surface area reducing the interfacial performance of PMMA [141, 152]. An illustration of the thermal conductance of pure PMMA and a composite of PMMA is presented in Figure 11.

Mazhar and Qarni [153] investigated the thermal conductivity of the prepared PVC/MXene nanoclusters using the conventional hot plate method with varying concentrations of MXene monolayer nanosheets. Noticeably, there is a significant improvement in the thermal conductivity of PVC/MXene nanoclusters as shown in Figure 12 (a & b). As previously stated, the thermal conductivity of polymer composites is determined by a variety of characteristics, including size, concentration, type, filler dispersion, and, most importantly, the presence of a thermal barrier between polymer chains [134]. Consequently, Figure 12(a) implies that the increase in the concentration of MXene causes a significant increase in the thermal conductivity of the PVC. The thermal conductive network is the prominent factor among other factors, that explains the enhancement of thermal conductivity of MXene/PVC nanoclusters [147]. Hence the continuous increase in the concentration of MXene improves the thermal conductance of the composite by filling the voids in the Polyvinyl chloride matrix and establishing a connection across the MXene flakes/polymeric medium reaching a percolation threshold [149]. Figure 12(b) schematically explains the presence or absence of a thermal conductance network formed all over the polymer matrix in pure PVC and PVC/MXene nanocluster following a reduced and increased lodging of MXene respectively. The affinity of the MXene with PVC and the Phonon scattering behavior of MXene are significant reasons for the increased thermal conductivity of the polymer composite[141, 150].

Cao, Deng [147] used solution blending to examine the thermal conductance (TC) of a poly (vinylidene fluoride) (PVDF)/MXene composite (Figure 13). The investigation found that PVDF clusters with different concentrations of MXene (0-5wt%) had improved thermal conductivity as compared to pure PVDF. It is noteworthy that the PDVF composite with 5wt% MXene had the highest thermal improvement. This is due to some variables, the first of which is that MXene monolayer nanosheets are evenly scattered within the PVDF matrix, increasing the proximity ratio between them. Second, MXene in the matrix offers nucleation size for the PVDF medium, which is critical for enhancing composites' TCs. Finally, the stage interfacial compactivity between the MXene and PDVF matrix decreases the boundary thermal resistance because of the high surface area of the MXene nanosheets and hydrogen surficial bonding between the PVDF matrixes.

High-thermal-conductivity and high thermal stability of MXene/PVA nanoclusters were prepared by Liu and Li [154]. The out-turn of the PVA matrix on MXene's heat characteristics is investigated. By providing strong Ti-O linkages and clinging to the surface of the MXene without a noticeable altering of the crystal structure, the polymer significantly improves the heat stability of the MXene. The TCs of pristine MXene and MXene/PVA composite are observed to be 55.8 and 47.6 W/(m·K), respectively, this is higher when compared with some metals and fewer 2-D materials.

Research on MXene-prepared conductive polymeric nanoclusters (MXCP) which include polyaniline (PANI), (poly(3,4-ethylene dioxythiophene): poly(styrene sulfonic acid)) (PEDOT:PSS), polypyrrole (PPy), with focus on personal thermal management (PTM), have been reported [155, 156]. The psychological perception of an individual regarding the degree of coldness and hotness of the environment is referred to as PTM [157, 158]. Thermal comfort must be balanced to sustain an individual's physiological and/or psychological well-being. Some reviews on MXCP composites focus on personal comfort devices, for example [145] lodged silicon unto Polypyrrole/MX-designed textile, prepared through in-situ polymerization, was employed for Joule heating. The prepared nanocluster textiles demonstrated an increased conductivity up to 1,000 (W/(m·K)) per 2.33 sq and retained a good conductivity after 1,000 cycles with thermal resistance ranging from 39 to 61 K/W. The high-quality thermally enhanced textile was used to create a self-heating fabric for personal heat management. It was observed that the MX-PPy-silicon decorated textile improved the joule heating property of the designed fabrics from 40 °C to 79 °C, which can be compared to the Joule

heater prepared with MXene functionalized montmorillonite [159]. Surprisingly, the constructed heater's durable effectiveness was ascertained when it showed a constant temperature of 57 °C for 3,600 seconds after attaining the saturation temperature. Such exceptional heating capability at such a low driving voltage could pave the way for the development of wearable and smart heating systems.

Not long ago, Jiang, Yuan [160], [161] fabricated PEDOT and MXene incorporated multi-task cotton garments, for personal heating applications. This was achieved through spray-coating and vapor phase polymerization techniques as illustrated in Figure 14. The surface temperature of the designed textile structure increased from 71 to 78 °C, when 9 V voltage was applied. Further increase in the voltage to 12V, results in a tremendous increase in surface temperature to 193 °C as shown in Figure 14 c.

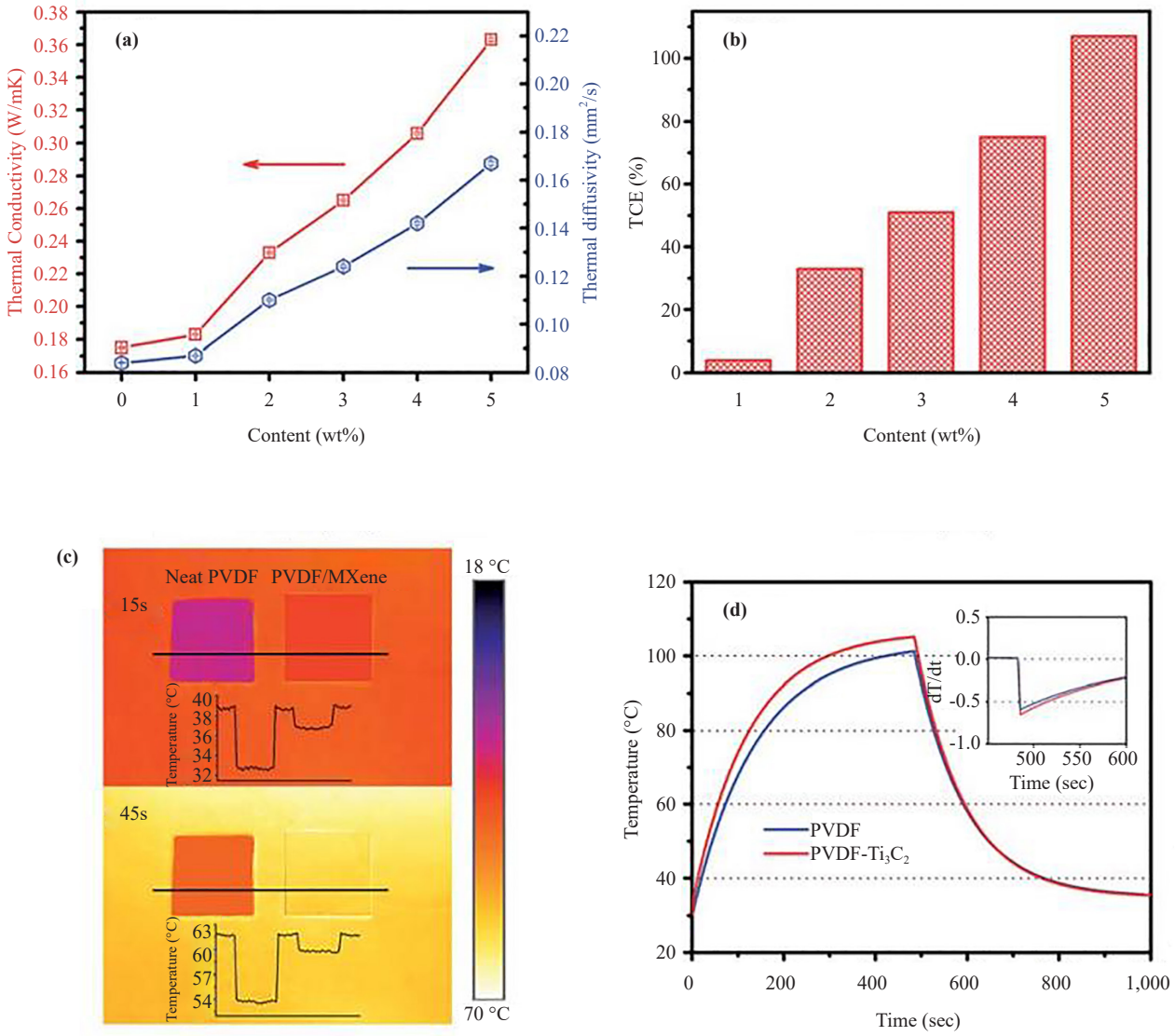

Figure 13. (a) effect of different fiber loading on the thermal diffusivity and thermal conductivity of PVDF composite (b) Thermal conductivity improvement of PVDF clusters compared to pristine PVDF. (c) Infrared images of pristine PVDF, and PVDF clusters with 5 wt% MXene, with 70 °C and 18 °C as the high and low temperatures respectively. (d) the varying surface temperature when heated and cooled, with 482 seconds as starting time. Reproduced with permission from Ref. [147]

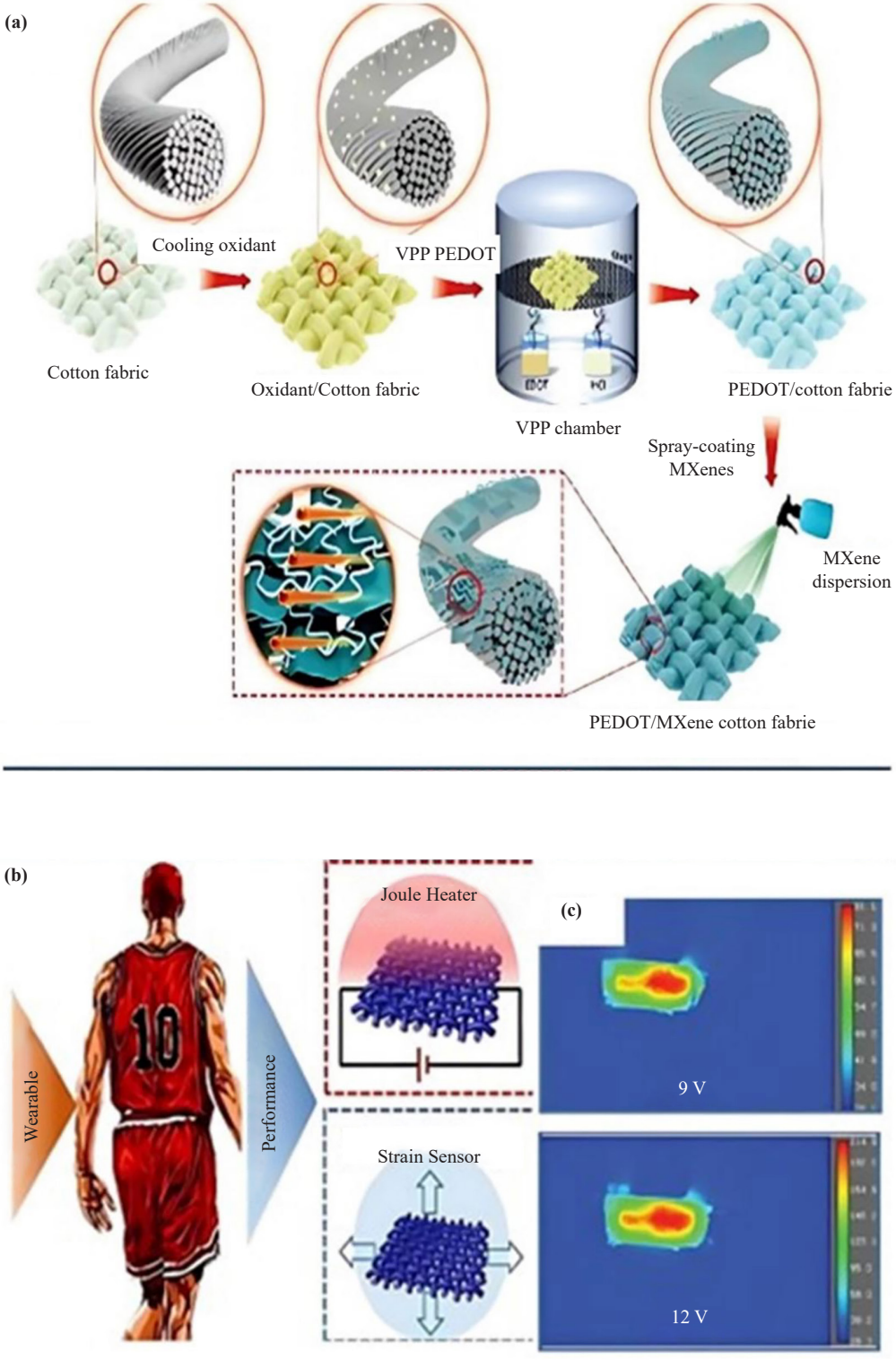

Figure 14 (a. and b.) Preparation and assembly of MXene-conductive polymer-coated multi-task fabrics, respectively [160]. (c) heating behavior of designed fabrics at varying inputted voltages [161].

5. Electrical properties of conductive MXene-polymeric hybrid nanoclusters

Regardless of the influence of surface groups, density functional theory demonstrates that pure MXenes have metal-like electrical conductivity [162]. Ascribable to the variability in the thickness, surface functionality, and layering tendency, MXenes have a variety of electronic characteristics which include metallic, energy storage, and semiconducting properties. The sorts of functional groups and their arrangement on the 2-D plane are related to the electrical structures of functionalized MXenes with -OH and -F exhibiting apparent semiconducting properties, according to theoretical simulations [162]. Depending on the synthesis and stacking procedure, MXenes have electrical conductivities ranging from 1 $S \cdot cm^{-1}$ to thousands of $S \cdot cm^{-1}$ [163]. Most studies on the electrical properties of MXene-polymeric nanoclusters are for electromagnetic interference shielding applications. $Ti_3C_2T_x$, the most widely researched MXene, has been integrated into many polymer matrices so far, because of their excellent layered structure and inherent electrical conductivity.

MXenes were deemed suitable nanosheets for creating multi-task and flexible fabrics [145]. Lodging in-situ polymerized PPy-loaded MXene flakes unto PET fabrics followed by a silicone coating resulting in a hydrophilic and highly electrically conductive textile. The resulting multifunctional fabric has an enhanced electrical conductivity of ≈ 1,000 Sm^{-1} when compared with pristine PPy-PET composite [123]. Following the strong quick-drying tendency of the fabric, the dependence of the composition of the polypyrrole/MXene hybrid in the textile and the electrical conductivity on the dip-coating cycle briskly increased with the dip-coating cycle number (Figure 15).

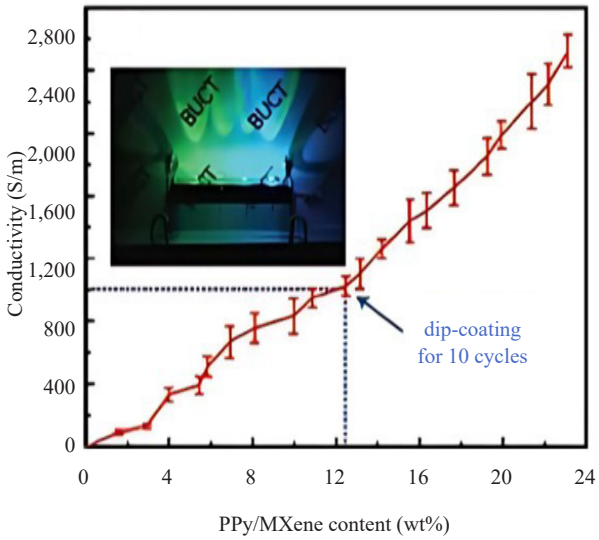

Figure 15. Plot of MXene-textile conductivity vs. Polypyrrole/MXene hybrid composition in textiles with varying dip-coating cycle numbers. Redrawn with permission from Ref. [145]

Utilizing a composite of $Ti_3C_2T_x$-MXene nano-flakes and poly (3, 4-ethylene dioxythiophene): polystyrene sulfonate, a one-step wet-spinning technique for fabricating highly conductive fibers was reported [7]. Fibers with a known electrical conductivity of ≈1,489 $S \cdot cm^{-1}$ were produced using this method. When MXene inclusion was raised to 30 wt%, the electrical conductivity of PEDOT:PSS fiber dropped to 548 ± 62 $S \cdot cm^{-1}$. The conductivity rose when the MXene loading was raised further, reaching a maximum value. These findings imply that at lower loadings (30 wt. %) of MXene, the conductivity of PEDOT:PSS dominated the fiber conductivity and that the loading of MXene-flakes disrupted the orderly packing of PEDOT, decreasing the fiber conductivity. The conductivity of MXene becomes more prominent at high MXene loading due to improved charge transport between MXene sheets. In another study, an unattached, flexible, and ultra-thin MXene/poly(3,4-ethylene dioxythiophene):poly(styrene sulfonate) (PEDOT:PSS) cluster film with a “stonework” structure was biomimetically designed and manufactured through a vacuum-assisted

filtering method [164]. The electrical conductivity of the polymeric cluster films fell dramatically as the PEDOT:PSS composition snowballed. The electrical conductivity of the pure MXene film was 1,000 S/cm, while the electrical conductivity of MXene to PEDOT:PSS was slowly reduced from 340.5 to 20.4 S/cm by reducing the MXene to PEDOT:PSS ratio from 7:1 to 3:1.

Following the fabrication of core-shell Fe_3O_4@PANI composites, vacuum-assisted filtration was used to create a lightweight and flexible MXene/Fe_3O_4@PANI cluster film with a burger-like intercalation architecture [165]. With more MXene, the electrical conductivities of the ultrathin nanoclusters with MXene nanosheets are enhanced. Utilizing hydrochloric acid and dodecylbenzene sulfonic acid (DBSA), polyaniline (PANI) was co-doped, and a few-layered MXene was produced using ionic intercalation and a sonication-employed technique [166]. Vacuum-assisted filtering was used to create MXene/co-doped PANI cluster films. The electrical conductivity improved as the mass fraction of MXene increased. The thickness of MXene/c-PANI cluster film was only 40 µm when the mass ratio of MXene to c-PANI was 7:1, and the electrical conductivity was dramatically increased to 24.4 $S \cdot cm^{-1}$ as a result.

The Resistance (R), resistivity (ρ), length (L), sheet resistance (Rs), and cross-section ($A = wt$; where w is width and t is thickness) can all be used to compute electrical conductivity (s). The resistance ($R = (\rho L)/A$) of the material is calculated using the arithmetic multiplication of resistivity and length divided by cross-section. The result of multiplying the values of Rs and t is the ρ [167]. The conductivities of nanoclusters made from the MXene-PAT-poly(p-aminophenol)-polyaniline copolymer were investigated by Raagulan et al. [168]. The electric conductivity (EC) of the MXene-PAT-poly (p-aminophenol)-polyaniline copolymer cluster was 7.0 $S \cdot cm^{-1}$. The nanoclusters of polyaniline (PANI), poly para-aminophenol (PpAP), PANI-PpAP, polythiophene (PTH), and Polypyrrole (PPy) polymers were also examined [168]. The thickness of the clusters ranged from 0.4 to 1.6 mm. Surface resistance and resistivity ranged from 1.6-160,000 Ω and 0.128-256,000 Ωcm, respectively, in the composites. The composites had conductivities ranging from 3.906×10^{-5} to 7.0 $S \cdot cm^{-1}$. In comparison to other composites, the MXene-PAT-PPY had a much higher resistance and resistivity, as well as an extremely poor electrical conductivity of 3.906×10^{-5} $S \cdot cm^{-1}$.

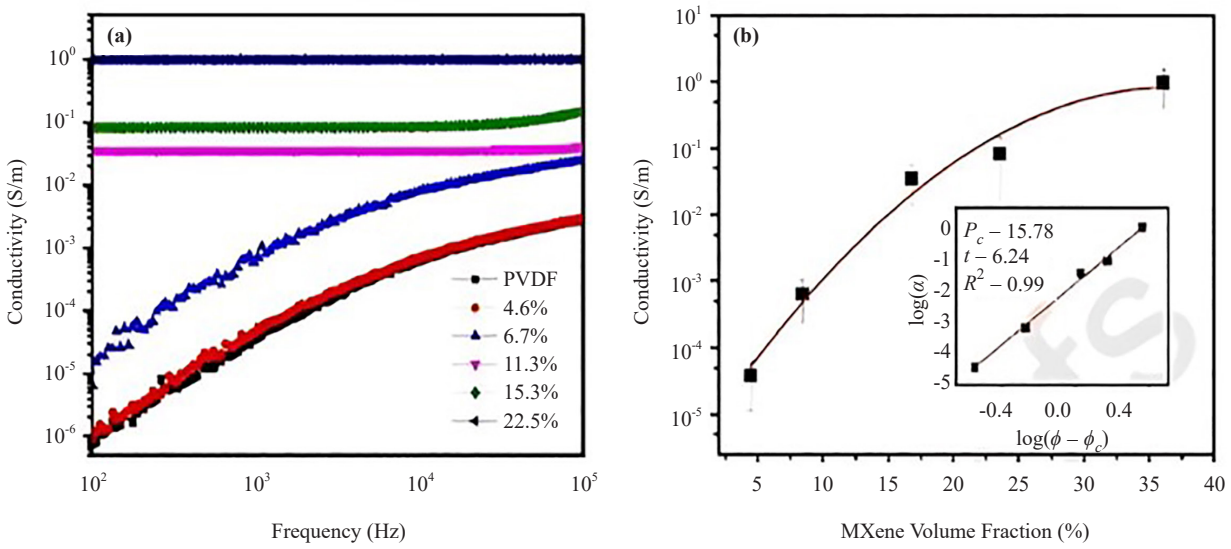

Figure 16. (a) electrical properties of MXene-polymer nanocomposites with varying volume fractions and frequency dependence. b) The effect of MXene filler loading on conductivity. Reproduced with permission from Elsevier [169]

The two-dimensional $Ti_3C_2T_x$ MXene/Polyvinylidene fluoride (PVDF) nanocomposites were tested for electrical conductivity [169]. The key challenge for effective electron transport in a non-conducting matrix is the arrangement of a well-connected conducting network with appropriate inclusion contents [170]. The AC electrical conductivity (σ_{AC}) of various concentrations of packed MXene lodged within the PVDF matrix was studied as a function of frequency (Figure 16a), and the elevated σ_{AC} after including different filler loading content was a result of the choosy localization of

MXene sheets in polymeric composite, whereas pristine PVDF demonstrates non-conductive behavior [171]. MXene-PVDF films' alternative current (AC) conductivity was measured as a function of frequency [172]. The AC electrical conductivity of every film enhanced in an almost transitional pattern as the frequency was increased. As expected, the highly conductive characteristic of MXene caused a rise in the AC conductivity of all uniform films when the MXene concentration was increased [173]. The increase in MXene volume fraction also increased the conductivity of the polymer nanocluster (Figure 16b).

Multilayered casting was used to create PVA/MXene films having an alternating multilayered structure [146]. The continual MXene sheet created a close network for electron conductivity. The PVA/MXene films with MXene contents of 7.5 wt%, 13.9 wt%, and 19.5 wt% exhibited electrical conductivities of 17, 379, and 716 $S \cdot m^{-1}$, respectively. The continual MXene sheet formed a connected conductive network, which contributed to the improvement of the electrical conductivity of the PVA/MXene multi-layered films. Furthermore, when the overall mass fraction of MXene grew, the thickness of the MXene sheet also increased. This allowed for the creation of a considerably effective conductive network throughout the film, resulting in increased electrical conductivity in the 13.9 and 19.5 wt% PVA/MXene films. Electrospinning was also used to successfully manufacture MXene-filled PVA nanofibers. The DC conductivity of PVA nanofibers containing 0.14 wt% MXene was 0.8 $mS \cdot cm^{-1}$ [174].

A simple freeze-drying process was used to create porous MXene/PVA cluster foams made of few-flaked MXene and PVA [175]. Due to the insulating holes being eliminated, the conductivity of the nanoclusters increased from 8.3×10^{-6} to 8.0×10^{-4} $S \cdot m^{-1}$. Electrostatic coupling of positive polystyrene microspheres with negative MXene nanoflakes, followed by compression molding, was demonstrated as a method for producing improved conductive MXene-polystyrene nanoclusters [176]. The resulting nanoclusters have a low percolation threshold of 0.26 vol % and a phenomenal conductivity of 1,081 $S \cdot m^{-1}$ thanks to MXenes' high conductivity and very efficient conducting network within the polystyrene matrix. In a different study, MXene was combined with either a charged poly-diallyl dimethylammonium chloride (PDDA) or an electrically neutral polyvinyl alcohol (PVA) [177]. The electrical conductivities of the MXene films were measured to be on the order of 2.4×10^5 $S \cdot m^{-1}$ using a typical four-probe approach, which is greater than carbon nanotube or graphene[178]. The as-prepared clusters were flexible and had electrical conductivities of up to 2.2×10^4 $S \cdot m^{-1}$ for the MXene/PVA cluster film, and the films comprising PDDA have a conductivity of up to 2,000 $S \cdot m^{-1}$. The inclusion of polymer chains between the $Ti_3C_2T_x$ sheets is thought to be the cause of the noticed decrease in conductivity when likened to pristine MXene films. Flexible polymer sheets, silicon, nylon fiber, stretchable poly (dimethyl siloxane), and glass were all effectively coated with MXene multilayers. MXene multilayer coatings that are conductive and conformal and can withstand bulk mechanical distortion while retaining a conductivity of up to 2,000 S/m have been reported [179].

Electrical conductivities of three-dimensional MXene/C hybrid foam/epoxy nanoclusters have been examined [180]. Ionic intercalation and sonication-assisted methods were employed to produce few-layered $Ti_3C_2T_x$ MXene, while sol-gel followed by thermal crushing was utilized to create porous three-dimensional MXene/C hybrid foam (MCF). Vacuum-enabled curing and impregnation methods were then employed to fabricate MCF/epoxy nanoclusters. The electrical conductivity of the nanocomposites was found to be highest at 184 $S \cdot m^{-1}$. Wang et al. looked into the electrical characteristics of heated MXene/Epoxy nanocomposites in another work [181]. Solution casting was used to create annealed MXene/epoxy nanoclusters. At lower concentrations, $Ti_3C_2T_x$ was randomly dispersed in the epoxy matrix, and MXene was frequently separated or enveloped by the epoxy matrix, hardly permitting them to come into touch with each other. As a result, forming efficient conductive networks was challenging, and electrical conductivities improved slowly. More contact with MXene could gradually create conductive networks as the mass fraction of MXene rose, resulting in enhanced electrical conductivities. The conductive networks of MXene-MXene became more efficient as the amount of MXene added increased, and the ability to conduct electrons increased as well, resulting in optimal electrical conductivity. The electrical conductivity of $Ti_3C_2T_x$/epoxy nanocomposites reached a maximum of 38 $S \cdot m^{-1}$ when the mass fraction of MXene was 15 wt%. The electrical conductivities of heated MXene/epoxy nanoclusters changed similarly to MXene/epoxy nanocomposites but at a faster rate. It had a higher electrical conductivity and a slower percolation threshold (Figure 17). The electrical conductivity of annealed MXene/epoxy nanocomposites reached up to 105 $S \cdot m^{-1}$ when the mass fraction of heated MXene was 15 wt%.

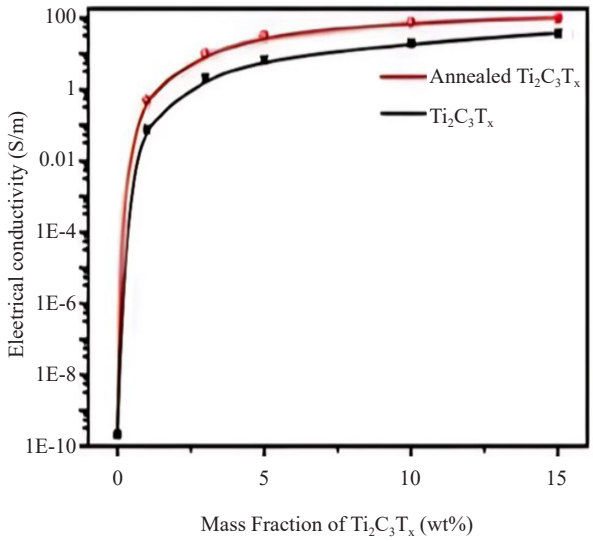

Figure 17. Electrical conductivities of the MXene/epoxy and heated MXene/epoxy nanocluster. Reproduced with permission from Elsevier [181]

Nanoclusters of graphene/MXene/epoxy (rGMH/epoxy) were developed [182]. To make the honeycomb structure rGO-MXene, an Al_2O_3 honeycomb was used as a template, and MXene was subsequently self-assembled on the rGH by electrostatic adsorption (rGMH). Through the addition of epoxy, rGMH/epoxy nanocomposites were successfully prepared. With the same MXene loading, the conductivity of rGMH/epoxy nanocomposites decreases as the honeycomb cell size grows. When using a cell size of 0.5 mm and 1.2 wt% rGO + 3.3 wt% MXene loading, much higher conductivity values (387.1 $S \cdot m^{-1}$) were obtained.

Following their remarkable metallic nature and electrical conductivity, MXenes are deemed attractive close substitutes to graphene. The hydrophilicity of MXene films, on the other hand, may have an impact on their reliability and stability when used in hydrated conditions. By stacking MXene flakes into films and then using a hydrazine-induced foaming technique, an efficient and simple method for fabricating hydrophobic, flexible, and freestanding MXene foam with optimum strength has been reported [183]. Contradicting the common hydrophilic MX materials, the MXene foams unexpectedly have excellent water-resisting surfaces and durability. The electrical conductivity of the MXene sheet was up to 400,000 $S \cdot m^{-1}$. The samples' thickness grew after foaming, whereas their electrical conductivities dropped. This was due to the insulating holes that had been inserted. Additionally, because of the high aspect ratio, large specific surface area, and enough terminated OH groups, 2-D MXene was prepared and used as a common inclusion. To ascertain the role of MXene on membrane microstructure and proton conduction properties, it was introduced into a polymer matrix. Membrane matrixes were made up of phase-separated and non-phase-separated (basic chitosan) polymers [184]. The membranes' proton conduction properties were investigated. It is shown that MXene has a considerable promotion effect on the membrane proton conduction by enabling both Grotthuss-type proton transfer and vehicle-type, resulting in multiple higher proton conductivity under varied conditions for all polymeric cluster membranes.

By creating linked MXene networks in the NR matrix, Luo et al. [185] established an effective vacuum-assisted filtering technique for the manufacture of highly conductive and flexible MXene/natural rubber (NR) nanoclusters. High electrical conductivities of polymer nanoclusters with low MX concentration remained a challenge. There is an insulator-to-conductor transition as the MXene concentration increases, and the fitting results gave the nanoclusters one of the lowest percolation thresholds of 0.91 vol%. Furthermore, for 3.10 vol% and 6.71 vol%, excellent electrical conductivities of 500 and 1,400 $S \cdot m^{-1}$ were attained, respectively. The usual transitional ohmic property of their I-V curves, as well as the higher gradients with increasing concentration, corroborated the increased electrical characteristics of the MXene/NR nanoclusters. Mayer Berger and colleagues prepared and analyzed polymer-MXene composite nanofibers [186]. Delaminated MXene flakes were electrospun with alginate/PEO, poly (acrylic acid) (PAA), poly (vinyl

alcohol) (PVA), and polyethylene oxide (PEO). The structure and characteristics of nanofibers with minor amounts of delaminated MXene (1% w/w) were compared and examined to those of pristine polymer nanofibers. The inclusion of MX enhanced the electrical conductivity of most polymer solutions. The conductivity of the 1% (w/w) MXene/PEO solution increased by 73.6% when compared to the conductivity of PEO alone. In comparison to their basic polymer solutions, 1% (w/w) MXene/PEO/alginate and 1% (w/w) MXene/PVA showed a 34.6% and 6.2% improvement in conductivity, respectively. The conductivity of the MXene/PAA solution at 1% (w/w) was essentially unaffected, with only a 0.9% drop. The conductivity data support the 1% (w/w) MXene/PAA solutions, indicating weak bonding between the two constituents.

The preparation and characterization of MXene-Polyacrylamide (PAM) nanocluster films were evaluated [187]. Inter-layering of dimethyl sulfoxide between MXene layers resulted in complete delamination of the MXene layers, resulting in a homogeneous distribution of solvent-resistant MXene nanoflakes in wet PAM solutions. Polymeric cluster solutions containing almost 75% polymer were synthesized. The conductivity of the as-fabricated cluster samples was improved greatly to 3.3×10^{-2} S·m^{-1} with only 6 wt% (1.7 vol%) MXene inclusion. Casting was used to create transparent, flexible, and electrically conductive thin nanocluster films based on a polyamide matrix functionalized with two-dimensional MXene nanoflakes [188]. The optimum reported electrical conductivity was 1.4×10^{-2} S·cm^{-1} for the cluster loaded with 5 wt% MXene, while the percolation threshold of the MXene inclusion within the PAM matrix was found to be 0.05 vol%. The as-fabricated MXene has an electrical conductivity of 9.1 S·cm^{-1}, while the MAX phase has a conductivity of 172 S·cm^{-1}.

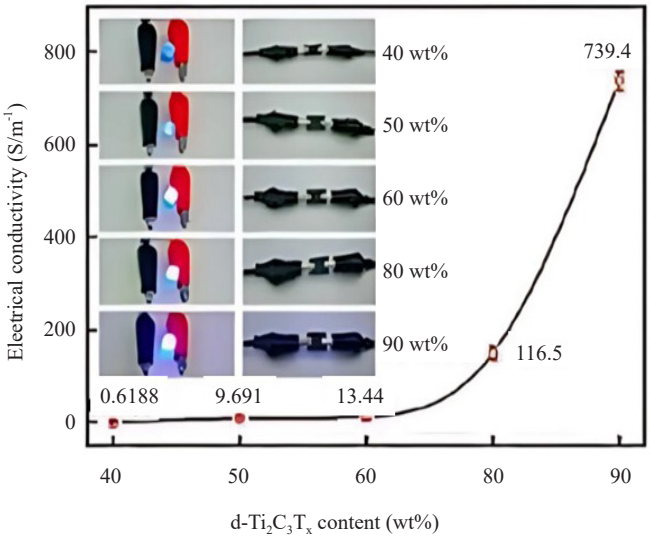

Figure 18. Plot of electrical conductivity versus d-$Ti_3C_2T_x$ inclusion for the d-$Ti_3C_2T_x$/CNF cluster paper flakes with varied d-$Ti_3C_2T_x$ inclusions. Reproduced with permission from Elsevier [170]

Conductive MXene/cellulose nanofiber (CNF) films were investigated by Zhan et al. [189]. By developing a well-established conductive channel, the composite paper's conductivity gradually rose as the MXene content grew. The electrical conductivity of the composite paper with 20 wt% MXene was 2.1 S·m^{-1}. An increase in MXene content gives additional opportunity for MXene nanoflakes to overlap in MXene/CNF composite sheets, resulting in better conductivity. With 50 wt% MXene loadings, an optimum conductivity of 2,837 S·m^{-1} was achieved. The causes for the composite papers' ideal conductivity were explained because of the extraordinarily high MXene loadings, which provided composite papers with effective conduction pathways. Secondly, the orientated alignment of 2-D MXene nanoflakes resulted in a flawless connection and a larger overlap area. Finally, 1-D CNFs resulted in reduced re-stacking between MXene nanoflakes. Sequel to the fast-increasing usage of electrical communication equipment, a vacuum-filtration-induced self-assembly approach was used to create flexible and ultrathin MXene (d-$Ti_3C_2T_x$,)/CNF cluster

paper with a nacre-like lamellar structure [190]. The electrical conductivity of the MXene/CNF cluster paper was 739.4 $S \cdot m^{-1}$ when the content of d-$Ti_3C_2T_x$ was 90 wt%, (Figure 18). The d-$Ti_3C_2T_x$ sample had an electrical conductivity of 1,142.5 $S \cdot m^{-1}$. The electrical conductivity of the d-$Ti_3C_2T_x$/CNF cluster paper decreased when likened to the d-$Ti_3C_2T_x$ sample because CNFs are an insulating polymer. Fortunately, when compared with the conventional dielectric polymers, the CNFs have a unique 1-D nanofiber structure, resulting in low non-conductive interactions with 2-D conductive d-$Ti_3C_2T_x$ nanoflakes. Furthermore, the vector arrangement of the 2-D d-$Ti_3C_2T_x$ nanoflakes along the planar direction can produce a conductive network, which assures the sufficient linkage of d-$Ti_3C_2T_x$ nanoflakes, thanks to the cohesive action of CNFs.

6. Capacitive energy storage applications of conductive MXene-MXene-polymeric hybrid nanoclusters

The extensive and unique physicochemical, mechanical, optical, electrochemical, and electronic properties of MXene and conducting polymers have drawn the attention of researchers. They are keen on designing high-performance energy storage clusters using these materials to address the growing demand in the technology sector for instant power supply to wearable electronics [64]. The use of conducting polymers alone is a well-developed technology but there are concerns with it in terms of practicability, prompting researchers to look for necessary modifications to the architecture for optimal performance. On the heels of this research adventure, MXene-based conducting polymeric hybrid nanoclusters were developed to simultaneously maximize the individual advantages of the two materials while making up for their inherent functional deficiencies. In this section, the recently emerging progress in the applications of conductive MXene-based polymeric hybrid nanoclusters in energy storage systems is elucidated. The preparation techniques and the electrochemical performance of the nanoclusters are also described. The discussions are based on the three MX-polymeric nanoclusters (MX-PPY, MX-PANI, and MX-PEDOT:PSS). This presents insight and a technological path for preparing high-capacitive MXene-PPy, MXene-PANI, and MXene-PEDOT:PSS clusters for applications in energy storage systems.

6.1 *Applications of MXene-Polyaniline (PANI) nanoclusters in energy storage devices*

PANI is a conducting polymer with an organically connected semiconducting chain that belongs to the semi-flexibility rod-like polymeric class. It exhibits exceptional temperature inhibition characteristics, mechanical and electrochemical properties, solubility in various types of solvents, and eco-benign stability [191, 192]. PANI is also known as aniline black and comes in a variety of forms depending on the degree of oxidation. Pernigraniline base refers to completely oxidized PANI; emeraldine base refers to partially oxidized PANI; and leucoemaraldine base refers to completely reduced PANI [192, 193]. PANI is a good conducting polymer owing to its ease of synthesis, tunable characteristics, high polymerization yield, inexpensiveness, and environmental stability. PANI has potential uses in energy storage, electrodes, EMI shielding, sensors, solar cells, and nonlinear optics, among others [192].

The creation of PANI-nanoclusters with inorganic nano-reinforcement like MXene is a promising strategy to improve PANI's performance and characteristics. This results in a nanocomposite that demonstrates appreciable synergistic/complementary characteristics. The applications of these nanoclusters are found in energy storage, LEDs, electrochromic gadgets, electrostatic discharge systems, batteries, EMI shielding, chemically and biochemically manufactured sensors, etc. [194]. However, the focus of this section is on its application in energy storage gadgets.

The fabrication of high electrochemical performance supercapacitor electrodes using a graphene-encapsulated MXene/polyaniline (GMP) composite has been studied by Fu et al. [195]. The GMP electrode so developed has enhanced cycle stability and electrochemical performance. It has a high gravimetric capacitance value of 635 $F \cdot g^{-1}$, and a volumetric capacitance of 1,143 $F \cdot cm^{-3}$ with exceptional cycling stability of 97.54% after 10,000 cycles at a current density of 1 $A \cdot g^{-1}$. Besides, the pouch-type asymmetric supercapacitor produced utilizing GMP as a positive electrode and graphene as a negative electrode has a high energy density value of 42.3 $Wh \cdot kg^{-1}$ at a power density of 950 $W \cdot kg^{-1}$ and excellent cycle stability of 94.25% after 10,000 cycles at 10 $A \cdot g^{-1}$.

In another study, the significance of high energy density, as well as improved capability rate in supercapacitors

for flexible electronics, was especially highlighted. PANI-NTs/MXene nanoarchitecture was synthesized through a facile and self-alignment of 1-D PANI nanofibrous polymer and 2-D MXene nanosheets providing hyper-elevated rate capability, highly improved specific capacitance (596.6 $F \cdot g^{-1}$ at 0.1 $A \cdot g^{-1}$), distinctive cyclability (94.7% after 5,000 cycles), optimum energy density (25.6 $Wh \cdot kg^{-1}$ at 153.2 $W \cdot kg^{-1}$), power density (1,610.8 $W \cdot kg^{-1}$ at 13.2 $Wh \cdot kg^{-1}$) and exceptional cycling stability (81.1% after 4,000 cycles) thus delivering valuable pathway for the design of energy storage gadgets that exhibit high power and energy densities [196].

Further, Layer-by-layer (LbL) coupling, which is based on the alternating adsorption of oppositely charged species to a surface to build a nanostructured electrode, has been identified by Yun, Echols [197] as a potential technique for developing ultrathin-film electrodes. Their work focused on the LbL formation of hybrid electrodes from positively charged polyaniline nanofibers (PNFs) and negatively charged 2-D MXene for thin-film energy storage gadgets. The coupling involved the deposition of PNFs and MXene in films of 49 nm/layer thickness. The content comprises 23 and 77 wt% of MXene and PNFs respectively. This resulted in a sandwich cell that gave an areal capacity of 17.6 $\mu A \cdot h \cdot cm^{-2}$, an energy of 22.1 $\mu W \cdot h \cdot cm^{-2}$, and a power of 1.5 $mW \cdot cm^{-2}$ for a 2 μm thickness of PNF/MXene multilayer. The work demonstrated that LbL PNF/MXene thin films could be employed as electrode materials in thin-film energy storage devices for wearable electronics. In another study by Zhou et al. [198], MXene/PANI composites were investigated as potential anode materials for sodium-ion batteries. The findings showed that the introduction of PANI effectively aided the suppression of the restacking as well as improved mechanical flexibility and electric conductivity. The introduction of PANI also aids in the preservation of high sodium adsorption strength and rapid sodium mobility, as well as the positive features associated with average open circuit voltage and maximum sodium content of MXenes. Based on these positive attributes, the authors suggested that MXene/PANI composites are potential anode choices for Na-ion batteries. Also, the utilization of MXene/PANI hybrid electrodes for the production of sophisticated supercapacitors through the hydrothermal reaction process has been reported by Li et al. [199]. With current densities ranging from 0.5 to 20 $A \cdot g^{-1}$, the 1:3 MXene/PANI electrode demonstrated high capacitance retention and specific capacity of 84.72% and 563 $F \cdot g^{-1}$ respectively. At the same MXene/PANI ratio of 1:3, it also exhibited a long usage cycle, with 95.15% capacitance retention after 10,000 cycles as well as energy and power densities of 22.67 Wh/kg and 0.217 kW/kg respectively.

In a different study, a novel nanocomposite of MXene/PANI decorated with graphene nanosheets has been fabricated by Wang et al. [200]. The fabricated nanocluster showed enhanced pseudocapacitive characteristics when utilized as a supercapacitor electrode, the graphene helps to inhibit the assemblage of the MXene single-layers and enables the uneven formation of PANI on the layered MXene structure. Besides, graphene helps to create more pathways for ions/electrons to flow between the electrodes and the electrolyte, acting as "conductive bridges." The results showed that the fabricated nanoarchitecture has an exceptional electrochemical performance way better than the reported MXene-based devices.

6.2 *Applications of MXene-Polypyrrole (PPy) nanoclusters in energy storage devices*

Polypyrrole is a conducting polymer that has sparked a lot of interest because of its unusual biocompatibility, ease of synthesis, and inherent high conductivity [192, 201]. Polypyrrole is an organically linked polymeric matrix created by oxidative pyrrole polymerization. Because of its potential electrochemical inclination, PPy has garnered a lot of interest in supercapacitor electrodes, but its electrochemical output has been limited by its poor cycle stability and tightly packed architecture [202]. To overcome the shortcomings of sole conducting PPy, the blending of PPy with MXenes is an attractive technique to enhance its electrochemical performance and mechanical stability by complementing each other's advantages [203, 204].

An unsymmetrical supercapacitor device operating with a voltage of 1.7 V and a 0.5 M Na_2SO_4 electrolyte has been fabricated using MXene/PPy composites [205]. An increased capacitance of 1.37 $F \cdot cm^{-2}$ was reported from the cyclic voltammetry (CV) results while the galvanostatic charge-discharge (GCD) data gave 1.18 $F \cdot cm^{2}$. A helpful technique for fabricating MXene/PPy composites was presented, allowing for their use in negative electrodes and enabling exceptional capacitive properties at an AML of 40 $mg \cdot cm^{-2}$. Upon the optimization of the negative electrode's composition and performance, an increased capacitance of 2.11 $F \cdot cm^{-2}$ and 2.49 $F \cdot cm^{-2}$ were obtained from the CV and GCD data, respectively while maintaining low electrode resistance.

Wei et al. [206] in their study demonstrated a simple technique to fabricate an MXene/PPy heterostructure nanocomposite as an improved electrode material for supercapacitors. 75 nm PPy nanospheres were attached to ultra-

thin MXene nanosheets through in situ polymerizations of PPy monomers at the input of MXene suspension. At a scan rate of 2 $mV \cdot s^{-1}$, the specific capacitance of the nanocomposite was 458 $F \cdot g^{-1}$, which was much higher than that of pure MXene (132 $F \cdot g^{-1}$). Also, the optimal MXene/PPy nanocluster demonstrated outstanding cycle stability. At a power density of 499.94 $W \cdot kg^{-1}$, the MXene/PPy supercapacitor delivered an elevated energy density of 21.61 $Wh \cdot kg^{-1}$. An initial capacitance retention value of 73.68% was obtained at $1A \cdot g^{-1}$ after 4,000 charge and discharge tests. Generally, the novel nanocluster (MXene/PPy) demonstrated stable microstructure and exceptional energy storage attributes and has good prospects for practical application in energy storage devices.

In a different study, monomers of pyrrole were in-situ polymerized under low temperatures to form evenly distributed PPy nanoparticles on organ-like MXene/PPy nanoflakes, resulting in a unique organ-like MXene/PPy nanocomposite [207]. The electrochemical properties and microstructures of the MXene/PPy composites were studied at different mass ratios. The organ-like MXene/PPy nanocluster demonstrated an optimum specific capacitance value of 184.36 $F \cdot g^{-1}$ at 2 $mV \cdot s^{-1}$ with unique cycling stability of about 83.33% at 1 $A \cdot g^{-1}$ after 4,000 cycles. The organ-like MXene configuration inhibits PPy development, reduces PPy stacking, and improves MXene/PPy nanocomposite structural stability. Furthermore, the intercalation of identical Polypyrrole nanoparticles increased the interlayer spacing of MXenes, and the well-aligned PPy polymer chains provide additional paths for the diffusion of the ions of the electrolyte and charge transfer, resulting in increased specific capacitance and lower charge transfer resistance. Above all, it presented a convenient and low-cost method for large-scale fabrication of MXene/Polypyrrole nanoclusters which have amazing properties and look interesting as a supercapacitor electrode material. More so, a simple and effective technique to fabricate MXene/PPy 3-D carambola-like composite film electrodes was developed *via* a single-step co-electro-deposition by Jian, He [127]. The 3-D composite configuration aided ionic diffusion and electron transfer, hence the MXene/Polypyrrole cluster film electrodes demonstrated excellent electrochemical attributes with an outstanding gravimetric capacitance of 416 $F \cdot g^{-1}$ at 0.5 $A \cdot g^{-1}$ current density.

Mani Mahajan and co-workers [208] used a simple synthetic approach to synthesize polypyrrole-encapsulated polyoxomolybdate (PMo_{12}) embellished with MXene as a novel potential 2-D/3-D nanosheets for a high-performance lithium-ion battery for energy storage. Sequel to the inherent self-assembly and electrostatic repulsion attributes of PMo_{12} anions, they (PMo_{12} anions) are wrapped by the discrete PPy molecules and aid in effective inter-placing between the layers of MXene. As a consequence, the composite electrode demonstrates an outstanding lithium storage capacity of about 764 $mAh \cdot g^{-1}$ at 0.1 $A \cdot g^{-1}$ and elongated cycling stability of about 2,000 cycles at 3 $A \cdot g^{-1}$ as well as remarkable rate performance. Because of the synergistic impact between PPy-encapsulated PMo_{12} and MX, this distinctive 2D/3D design shows a hybrid battery-capacitive attribute. The reversible redox reactions of PMo_{12} are responsible for the battery component while PPy and MXene provide for the pseudocapacitive component.

To further demonstrate the benefits of incorporating conducting PPy on MXene in energy storage systems, Yan et al. [209] used MXene nanosheets following a facile "dipping and drying" technique to obtain conductive textile electrodes whose specific capacitance value (182.70 $F \cdot g^{-1}$) was higher than the values reported for active carbon and carbon nanotubes. When conducting Polypyrrole was deposited (electrochemically) on the surface of MXene textiles, a Polyoyrrole/MXene composite textile electrode with a specific capacitance value of 343.20 $F \cdot g^{-1}$ was obtained. Also, a symmetrical PPy-MXene textiles-based supercapacitor with an energy density of 1.30 $mW \cdot h \cdot g^{-1}$ (power density, 41.1 $mW \cdot g^{-1}$) was assembled. The work presented a novel MXene-based textile supercapacitor that is promising for utilization in the assembling of wearable energy storage devices.

6.3 *Applications of MX-Poly (3, 4-ethylene dioxythiophene):Polystyrene Sulfonate (PEDOT:PSS) nanoclusters in energy storage devices*

PEDOT:PSS is the product of the doping of poly(3,4-ethylene dioxythiophene) (PEDOT) with poly(styrene sulfonate) (PSS) [210]. It is a polymeric blending of dual ionomeric configurations [192, 211]. The fabrication of PEDOT:PSS is accomplished by mixing an aqueous solution of PSS with an EDOT monomeric unit, then adding a sodium persulfate and ferric sulfate solution to the resulting blend [212]. PEDOT:PSS finds its utilization in different areas of conductive organic thermoelectrical architectures such as in thermoelectrical generators, however, the majority of its applications are centered on transparent, conductive polymeric units with maximum ductility [192, 213]. In organic bioelectronics, PEDOT:PSS is the most widely utilized conducting polymer [210]. Nevertheless,

electrochemical capacitances surpassing what is currently provided by the existing conducting polymers are required for state-of-the-art electronic and energy storage devices. Also, there are concerns over the long-term durability of sole-conducting polymer films in aquatic environments during device operation and storage [210]. To this end, the blending of PEDOT:PSS with MXene to form a nanocluster that maximizes their unique advantages while complementing their shortfalls has recently received special attention from researchers.

To demonstrate the practical application of MXene/PEDOT:PSS nanocluster in energy storage devices, a tartaric acid-treated, MXene/PEDOT:PSS composite was prepared and used as electrodes for ultra-fast supercapacitor as depicted in Figure 19. Among all other 2-D nanoclusters, the MXene/PEDOT:PSS-based supercapacitor offers outstanding performance in alternating current (AC) filtering applications [214].

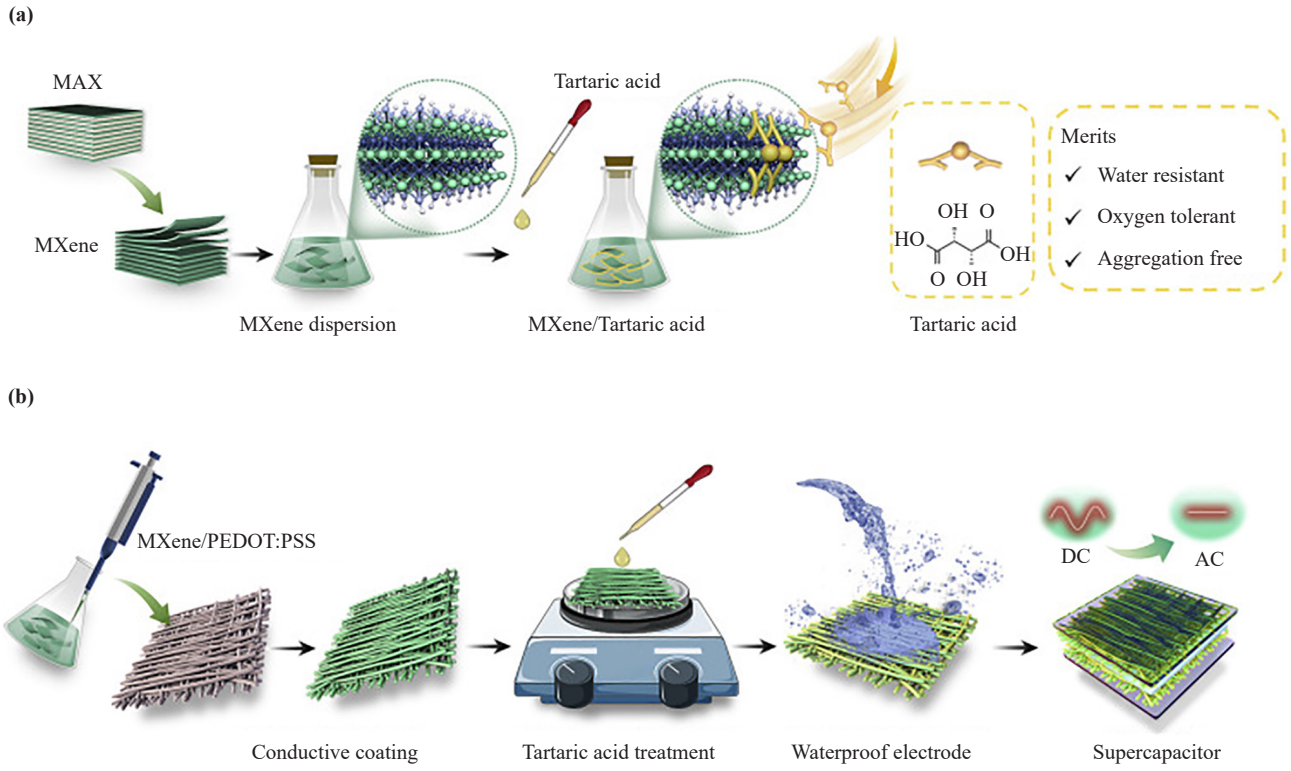

Figure 19. Schematics of the processing procedure of an ultrafast supercapacitor using a tartaric acid-treated, MXene/PEDOT:PSS composite. (a) chemically stabilized MXene aided by tartaric acid; (b) structurally stabilized MXene/PEDOT:PSS cluster coating for fabrication of supercapacitor. Reproduced with permission from Elsevier [214]

Further, the electrochemical synthesis of MXene/PEDOT:PSS composite has been reported by Wustoni, Saleh [210]. It was discovered that the incorporation of PEDOT:PSS in the MXene architecture results in films with unusually high stability (capacitance retention = 78.44 ± 1.75% over 500 cycles) and volumetric capacitance (607.0 ± 85.3 $F \cdot cm^{-3}$), better than sole PEDOT:PSS films fabricated under the same process conditions. In another study, Li, Zhang [215] introduced a facile and plausible technique to fabricate flexible MXene/PEDOT:PSS films with remarkable volumetric capacitance for unsymmetrical supercapacitors. The method involved filtering the MXene/Clevios compound inks, this was proceeded by sulphuric acid treatment. The acid treatment helps to eliminate the portion of the non-conducting PSS from the MXene/PEDOT:PSS composite film, leading to an important improvement in the conductivity of the cluster. Besides acting as a bridge between MXene sheets to expose further electroactive surfaces and minimize the pathways for ion diffusion, conductive PEDOT also served as a conductive network, forming thousands of dimensional electronic transport routes for speeding up the electrochemical interaction process. Consequently, the synthesized

MXene/PEDOT:PSS-100-H composite film demonstrated a 4.5-fold rise in the specific surface area with greater rate performance, as well as outstanding volumetric capacitance (1,065 $F \cdot cm^{-3}$ at 2 $mV \cdot s^{-1}$). The composite film electrode showed significant potential for utilization as a robust power source for smart wearable electronic gadgets.

More so, a high-performance, very-thin, wearable supercapacitor was developed based on a layered structure of $Mo_{1.33}C$ MXene/PEDOT:PSS hybrid film with concentrated sulphuric acid posttreatment. The smart flexible supercapacitor offers an optimum capacitance (568 $F \cdot cm^{-3}$), high energy density, and power density of 33.2 $mWh \cdot cm^{-3}$ and 19,470 $mW \cdot cm^{-3}$ respectively. When treated with H_2SO_4, the prepared hybrid film demonstrated a decrease in resistance, increased capacitance (1,310 $F \cdot cm^{-3}$), and enhanced rate abilities than the $Mo_{1.33}C$ MXene/PEDOT:PSS hybrid films that were not H_2SO_4 treated [216].

On the other hand, owing to their appreciable low cost, energy density, and environmental friendliness, lithium-sulfur (Li-S) batteries have generated a lot of interest. However, the severe shuttle effect associated with Li-S batteries remains an impediment to its practical application. An effective approach to remedy this challenge is to formulate a modified separator as the second collector using conductive and polar materials. To this end, Li et al. [217] fabricated an MXene/PEDOT:PSS composite for the modification of PP separators. The use of MXene/PEDOT:PSS makes MXene nano-sheets efficiently anchor polysulfide, thereby preventing the shuttle effect. Hence, Li-S batteries with MXene/PEDOT:PSS filled-separators show highly improved performances, such as low decay rate and elongated cycling stability (0.030%/cycle at 0.5 C) after 1,000 cycles, and high discharge capacity (1,241.4 $mA \cdot h \cdot g^{-1}$ at 0.2 C). In a further response to the need for future electrodes for wearable electronics, a new blend of the silver nanowire (AgNW) MXene/PEDOT:PSS (AgNW- MXene@PEDOT:PSS) was fabricated through a solution blending [218]. Bonding between MXene and PEDOT:PSS aids a high conductive AgNW- MXene@PEDOT:PSS realizes a sheet resistance and transmittance of 17 $\Omega \cdot sq^{-1}$ and 97.6% respectively, as well as enhances stability and anti-corrosion attribute. It proposed an essential step toward the fabrication of nanoclusters for flexible smart electronics.

Table 1. Summary of MXene/conductive polymeric nanoclusters, application, and performance in energy storage

Nanocomposite	Application	Performance	References
Graphene-encapsulated MXene/PANI (GMP)	Asymmetric Supercapacitor (ASC)	Gravimetric capacitance, 635 $F \cdot g^{-1}$; Volumetric capacitance, 1,143 $F \cdot cm^{-3}$ at 1 $A \cdot g^{-1}$; Cyclability, 97.54% after 10,000 cycles; Energy density, 42.3 $Wh \cdot kg^{-1}$; Power density, 950 $W \cdot kg^{-1}$.	[195]
MXene/PANI Nanotubes (PNTs)	Symmetric supercapacitors (SSC)	Specific capacitance, 596.6 $F \cdot g^{-1}$ at 0.1 $A \cdot g^{-1}$; Cyclability, 94.7% after 5,000 cycles; Energy density, 25.6 $Wh \cdot kg^{-1}$ at 153.2 $W \cdot kg^{-1}$; Power density, 1,610.8 $W \cdot kg^{-1}$ at 13.2 $Wh \cdot kg^{-1}$.	[196]
M MXene/PANI Nanofibers (PNFs)	Thin-film electrodes (microbatteries)	Areal capacity, 17.6 $\mu A \cdot h \cdot cm^{-2}$; Energy, 22.1 $\mu W \cdot h \cdot cm^{-2}$; Power, 1.5 $mW \cdot cm^{-2}$.	[197]
MXene/PANI	Sodium-ion batteries	NA	[198]
MXene/PANI	Asymmetric supercapacitors (ASC)	Specific capacity, 563 $F \cdot g^{-1}$ at 0.5 $A \cdot g^{-1}$; Cyclability, 95.15% after 10,000 cycles; Energy density, 22.67 Wh/kg; Power density, 0.217 kW/kg.	[199]
Graphene-decorated MXene/PANI (GMP)	Asymmetric supercapacitor (ASC)	Gravimetric capacitance, 452 $F \cdot g^{-1}$; Volumetric capacitance, 606 $F \cdot cm^{-3}$; Rate capability, 79.6%; Cyclability, 80.4% after 5,000 cycles.	[200]
MXene/PANI	Supercapacitor (SC)	Gravimetric capacitance, 503 $F \cdot g^{-1}$; Volumetric capacitance, 1,682 $F \cdot cm^{-3}$; Cyclability, 98.3% after 10,000 cycles.	[219]

Table 1. (cont.)

Nanocomposite	Application	Performance	References
MXene/PPy	Asymmetric supercapacitor (ASC)	Volumetric capacitance, 2.11 $F \cdot cm^{-3}$; Gravimetric capacitance, 49 $F \cdot g^{-1}$; Low electrode resistance.	[205]
MXene/PPy	Supercapacitor (SC)	Specific capacitance, 458 $F \cdot g^{-1}$; Power density, 499.94 $W \cdot kg^{-1}$; Energy density, 21.61 $Wh \cdot kg^{-1}$; Cyclability, 73.68% after 4,000 cycles.	[206]
MXene/PPy	A supercapacitor (SC)	Specific capacitance, 184.36 $F \cdot g^{-1}$; Cycling stability, 83.33% after 4,000 cycles.	[207]
MXene/PPy	Symmetric supercapacitors (SSC)	Gravimetric capacitance, 416 $F \cdot g^{-1}$; Cyclability, 86.4% after 5,000 cycles.	[127]
PPy-encapsulated polyoxomolybdate (PMo_{12})/MXene	Lithium-ion battery	Lithium storage capacity, 764 $mAh \cdot g^{-1}$; Cycling stability, 2,000 cycles at 3 $A \cdot g^{-1}$.	[208]
PPy/MXene	Symmetrical textiles-based supercapacitor	Specific capacitance, 343.20 $F \cdot g^{-1}$; Energy density, 1.30 $mW \cdot h \cdot g^{-1}$; Power density, 41.1 $mW \cdot g^{-1}$.	[209]
Tartaric acid-treated MXene/PEDOT:PSS	Ultrafast supercapacitor (UFSC)	Areal capacitance (C_A), 1,149 $\mu F \cdot cm^{-2}$; Phase angle, 80° at 120 Hz.	[214]
MXene/PEDOT:PSS	Organic bioelectronics (neural electrodes)	Volumetric capacitance, 607.0 ± 85.3 $F \cdot cm^{-3}$; Cyclability, 78.44 ± 1.75% after 500 cycles.	[210]
MXene/PEDOT:PSS	Asymmetric supercapacitor (ASC)	Volumetric capacitance, 1,065 $F \cdot cm^{-3}$; A 4.5-fold rise in the specific surface area.	[215]
$Mo_{1.33}C$ MXene/PEDOT:PSS	Ultrathin Flexible Solid-State Supercapacitor	Specific capacitance, 1,310 $F \cdot cm^{-3}$; Energy density 33.2 $mWh \cdot cm^{-3}$; Power density, 19,470 $mW \cdot cm^{-3}$.	[216]
MXene/PEDOT:PSS	Lithium-sulfur (Li-S) battery	Cycling stability and decay rate, 0.030% per cycle at 0.5 C after 1,000 cycles; Discharge capacity, 1,241.4 $mA \cdot h \cdot g^{-1}$ at 0.2 C.	[217]

7. Conclusion

The growing demand for smart and flexible electronics has driven researchers to seek necessary modifications to these architectures to enhance their performance. Due to the remarkable synergistic effects between materials in designed hierarchical structures, composite materials often exhibit enhanced physical and chemical properties. This underscores their potential for significant advancements in electrochemical attributes and high performance in wearable electronic devices. MXene/conducting polymeric hybrid nanoclusters were developed to simultaneously maximize the individual advantages of the two materials while making up for their inherent functional deficiencies. Herein, the electronic and thermal behaviors of conductive MXene-$Ti_3C_2T_x$-based polymeric composites and their capacitive energy storage applications are presented (Table 1).

The thermal properties of the composites are influenced by various factors such as the size, concentration, type, dispersion of fillers, and the presence of a thermal barrier between polymer chains. This survey revealed that the concentration of MXene significantly impacts thermal conductivity. Higher MXene concentration in the polymer matrix enhances both the thermal conductance and stability of the polymer nanocomposite. This effect is attributed to MXene's ability to form a thermal conductive network by establishing hydrogen bonds with the polymer, facilitating smooth heat flow within the composite. Additionally, strong interfacial compatibility between MXene and the polymer matrix, along with the phonon scattering nature of MXene nanosheets, contribute to the improved thermal conductivity and stability of conductive MXene/polymer hybrid nanoclusters.

The electrical conductivity of MXene-polymer nanoclusters is highly dependent on the ability of MXene to form an effective conductive network within the polymeric nanoclusters. The more efficient the MX-MX conductive network becomes, the better the electron transport within the nanoclusters. Additionally, metal nanoparticles such as Ag and Fe on functionalized MXene have been beneficial to the electrical conductivity of nanoclusters. Conductivity has been found to increase with the addition of metal particles in MXene nanoclusters.

Conclusively, it is important to note that while the use of standalone 2-D MXene in energy storage devices is a growing trend, the application of conducting polymers is a well-established technology. The practical applications of MXene/PANI, MXene/PPy, and MXene/PEDOT:PSS in energy storage devices as well as the preparation techniques were extensively discussed in this review. The work also elucidated the routes for exploring the enormous potential of MXene/conducting polymeric nanocomposites as one of the most promising state-of-the-art energy storage materials for smart, wearable, and flexible electronic applications.

Conflict of interest

The authors declare no competing financial interest.

References

[1] Folorunso O, Ajayi E, Akintelu S, Akinsola E, Ogunjimi I, Nwankwo H. Synthesis methods of borophene, graphene-loaded polypyrrole nanocomposites and their benefits for energy storage applications: A brief overview. *FlatChem*. 2021; 26: 100211.

[2] Kim HG, Lee HB. Atomic layer deposition on 2D materials. *Chemistry of Materials*. 2017; 29(9): 3809-3826.

[3] Naguib M, Kurtoglu M, Presser V, Lu J, Niu J, Heon M, et al. Two-dimensional nanocrystals produced by exfoliation of Ti_3AlC_2. *Advanced Materials*. 2011; 23(37): 4248-4253. Available from: https://doi.org/10.1002/adma.201102306.

[4] Das P, Wu Z-S. MXene for energy storage: present status and future perspectives. *Journal of Physics: Energy*. 2020; 2(3): 032004.

[5] Carey M, Barsoum MW. MXene polymer nanocomposites: A review. *Materials Today Advances*. 2021; 9: 100120. Available from: https://doi.org/10.1016/j.mtadv.2020.100120.

[6] Huang Y, Liang F, He Y, Zhang Z, Zhang S. Tailoring the electrical and thermal conductivity of multi-component and multi-phase polymer composites. *International Materials Reviews*. 2020; 65(3): 129-163.

[7] Zhang L, Deng H, Fu Q. Recent progress on thermal conductive and electrical insulating polymer composites. *Composites Communications*. 2018; 8: 74-82.

[8] Xu G, McGrath PB. Electrical and thermal analysis of polymer insulator under contaminated surface conditions. *IEEE Transactions on Dielectrics and Electrical Insulation*. 1996; 3(2): 289-298. Available from: https://doi.org/10.1109/94.486781.

[9] Xu X, Zhang Z, Li L, Wang W, Chen C, Zhao Z. Thermal conductivity of polymers and their nanocomposites. *Advanced Materials*. 2018; 30(17): 1705544.

[10] Chen J, Zhang Z, Li L, Wang W, Liu L, Zhao Z. Highly thermally conductive yet electrically insulating polymer/boron nitride nanosheets nanocomposite films for improved thermal management capability. *ACS Nano*. 2018; 13(1): 337-345.

[11] Wang D, Zhang Z, Li L, Wang W, Chen C, Zhao Z. Multifunctional 3D-MXene/PDMS nanocomposites for electrical, thermal and triboelectric applications. *Composites Part A: Applied Science and Manufacturing*. 2020; 130: 105754.

[12] Sun R, Zhou Y, Huang X, Yin F, Cheng L. Highly conductive transition metal carbide/carbonitride (MXene)@polystyrene nanocomposites fabricated by electrostatic assembly for highly efficient electromagnetic interference shielding. *Advanced Functional Materials*. 2017; 27(45): 1702807.

[13] Aakyiir M, Zhang Z, Li L, Wang W, Liu L, Chen J, et al. Elastomer nanocomposites containing MXene for mechanical robustness and electrical and thermal conductivity. *Nanotechnology*. 2020; 31(31): 315715.

[14] Xu MK, Li L, Zhang Z, Wang W, Chen J, Zhao Z. Electrically conductive $Ti_3C_2T_x$ MXene/polypropylene nanocomposites with an ultralow percolation threshold for efficient electromagnetic interference shielding.

Industrial & Engineering Chemistry Research. 2021; 60(11): 4342-4350.
[15] Mazhar S, Khan A, Ahmed A, Ghaffar A, Maqsood M, Iqbal N. Promising PVC/MXene based flexible thin film nanocomposites with excellent dielectric, thermal and mechanical properties. *Ceramics International*. 2020; 46(8): 12593-12605.
[16] Liu L, Zhang Z, Li L, Wang W, Chen J, Zhao Z. Functionalizing MXene towards highly stretchable, ultratough, fatigue-and fire-resistant polymer nanocomposites. *Chemical Engineering Journal*. 2021; 424: 130338. Available from: https://doi.org/10.1016/j.cej.2021.130338.
[17] Aghamohammadi H, Amousa N, Eslami-Farsani R. Recent advances in developing the MXene/polymer nanocomposites with multiple properties: A review study. *Synthetic Metals*. 2021; 273: 116695.
[18] Si JY, Yang K, Wu D, Wu K, Cao L, Wang X, et al. Functionalization of MXene nanosheets for polystyrene towards high thermal stability and flame retardant properties. *Polymers*. 2019; 11(6): 976.
[19] Chen X, Que W, Zhang L, Yin Z, Que M, Zhang F. MXene/polymer nanocomposites: preparation, properties, and applications. *Polymer Reviews*. 2021; 61(1): 80-115.
[20] George SM, Kandasubramanian B. Advancements in MXene-polymer composites for various biomedical applications. *Ceramics International*. 2020; 46(7): 8522-8535.
[21] Riazi H, Zamanian M, Javanbakht S, Ahmadi R, Ghaffarinejad A, Taghizadeh M, et al. Ti_3C_2 MXene-polymer nanocomposites and their applications. *Journal of Materials Chemistry A*. 2021; 9(13): 8051-8098.
[22] Riazi H, Taghizadeh G, Soroush M. MXene-based nanocomposite sensors. *ACS Omega*. 2021; 6(17): 11103-11112.
[23] Kumar D, Sharma RC. Advances in conductive polymers. *European Polymer Journal*. 1998; 34(8): 1053-1060.
[24] Nezakati T, Seifalian A, Tan A, Seifalian AM. Conductive polymers: Opportunities and challenges in biomedical applications. *Chemical Reviews*. 2018; 118(14): 6766-6843.
[25] Jonas F, Heywang G. Technical applications for conductive polymers. *Electrochimica Acta*. 1994; 39(8-9): 1345-1347.
[26] Shi Y, Wang J, Wang C, Zeng H, Deng Y. Nanostructured conductive polymers for advanced energy storage. *Chemical Society Reviews*. 2015; 44(19): 6684-6696.
[27] Kaur G, Adhikari R, Cass P, Bown M, Gunatillake P. Electrically conductive polymers and composites for biomedical applications. *RSC Advances*. 2015; 5(47): 37553-37567.
[28] Kiess HG, Baeriswyl D. *Conjugated Conducting Polymers*. Berlin: Springer-Verlag; 1992.
[29] Vilela F, Zhang K, Antonietti M. Conjugated porous polymers for energy applications. *Energy & Environmental Science*. 2012; 5(7): 7819-7832.
[30] Chauhan NP, Jadoun S, Rathore BS, Barani M, Zarrintaj P. Redox polymers for capacitive energy storage applications. *Journal of Energy Storage*. 2021; 43: 103218.
[31] Gurunathan K, Murugan AV, Marimuthu R, Mulik UP, Amalnerkar DP. Electrochemically synthesised conducting polymeric materials for applications towards technology in electronics, optoelectronics and energy storage devices. *Materials Chemistry and Physics*. 1999; 61(3): 173-191.
[32] Bryan AM, Santino LM, Lu Y, Acharya S, D'Arcy JM. Conducting polymers for pseudocapacitive energy storage. *Chemistry of Materials*. 2016; 28(17): 5989-5998.
[33] Pan L, Qiu H, Dou C, Li Y, Pu L, Xu J, et al. Conducting polymer nanostructures: Template synthesis and applications in energy storage. *International Journal of Molecular Sciences*. 2010; 11(7): 2636-2657.
[34] Xuan Y, Liu X, Desbief S, Leclère P, Fahlman M, Lazzaroni R, et al. Thermoelectric properties of conducting polymers: The case of poly (3-hexylthiophene). *Physical Review B*. 2010; 82(11): 115454.
[35] Ihnatsenka S, Crispin M, Zozoulenko IV. Understanding hopping transport and thermoelectric properties of conducting polymers. *Physical Review B*. 2015; 92(3): 035201.
[36] Bubnova O, Berggren M, Crispin X. Tuning the thermoelectric properties of conducting polymers in an electrochemical transistor. *Journal of the American Chemical Society*. 2012; 134(40): 16456-16459.
[37] Wang S, Sun H, Ail U, Vagin M, Persson PO, Andreasen JW, et al. Thermoelectric properties of solution-processed n-doped ladder-type conducting polymers. *Advanced Materials*. 2016; 28(48): 10764-10771.
[38] Toshima N, Ichikawa S. Conducting polymers and their hybrids as organic thermoelectric materials. *Journal of Electronic Materials*. 2015; 44(1): 384-390.
[39] Culebras M, Uriol B, Gómez CM, Cantarero A. Controlling the thermoelectric properties of polymers: Application to PEDOT and polypyrrole. *Physical Chemistry Chemical Physics*. 2015; 17(23): 15140-15145.
[40] Ezika AC, Sadiku ER, Idumah CI, Ray SS, Adekoya GJ, Odera RS. Recently emerging trends in MXene hybrid conductive polymer energy storage nanoarchitectures. *Polymer-Plastics Technology and Materials*. 2022; 61(8): 1-27. Available from: https://doi.org/10.1080/25740881.2022.2029888.
[41] Ezika AC, Sadiku ER, Idumah CI, Ray SS, Hamam Y. On energy storage capacity of conductive MXene hybrid

nanoarchitectures. *Journal of Energy Storage*. 2022; 45: 103686.
[42] Xu J, Hu X, Wang X, Wang X, Ju Y, Ge S, et al. Low-Temperature pseudocapacitive energy storage in $Ti_3C_2T_x$ MXene. *Energy Storage Materials*. 2020; 33: 382-389.
[43] Huang YH, Cheng WL, Zhao R. Thermal management of Li-ion battery pack with the application of flexible form-stable composite phase change materials. *Energy Conversion and Management*. 2019; 182: 9-20.
[44] Filho FGR, Mélo TJA, Rabello MS, Silva SML. Thermal stability of nanocomposites based on polypropylene and bentonite. *Polymer Degradation and Stability*. 2005; 89(3): 383-392. Available from: https://doi.org/10.1016/j.polymdegradstab.2004.12.011.
[45] Pielichowski K, Leszczyńska A, Njuguna J. Mechanisms of thermal stability enhancement in polymer nanocomposites. *Optimization of Polymer Nanocomposite Properties.* 2009; 9: 4.
[46] Xiao M, Sun L, Liu J, Li Y, Gong K. Synthesis and properties of polystyrene/graphite nanocomposites. *Polymer*. 2002; 43(8): 2245-2248.
[47] Liu R, Li W. High-thermal-stability and high-thermal-conductivity $Ti_3C_2T_x$ MXene/poly (vinyl alcohol) (PVA) composites. *ACS Omega*. 2018; 3(3): 2609-2617.
[48] Li L, Fu X, Chen S, Uzun S, Levitt AS, Shuck CE, et al. Hydrophobic and stable MXene-polymer pressure sensors for wearable electronics. *ACS Applied Materials & Interfaces*. 2020; 12(13): 15362-15369.
[49] Duquesne S, Le Bras M, Bourbigot S, Delobel R, Camino G, Eling B, et al. Thermal degradation of polyurethane and polyurethane/expandable graphite coatings. *Polymer Degradation and Stability*. 2001; 74(3): 493-499.
[50] Cerezo FT, Preston CML, Shanks RA. Structural, mechanical and dielectric properties of poly (ethylene-co-methyl acrylate-co-acrylic acid) graphite oxide nanocomposites. *Composites Science and Technology*. 2007; 67(1): 79-91.
[51] Jena DP, Malik R, Parida RK, Parida BN, Nayak NC. Thermal and dielectric behavior of $Ti_3C_2T_x$ (MXene) incorporated ethylene vinyl acetate copolymer/linear low-density polyethylene nanocomposites. *Journal of Materials Science: Materials in Electronics*. 2022; 33(7): 4278-4290.
[52] Chen F, Tao NJ. Electron transport in single molecules: From benzene to graphene. *Accounts of Chemical Research*. 2009; 42(3): 429-438.
[53] Sokol M, Natu V, Kota S, Barsoum MW. On the chemical diversity of the MAX phases. *Trends in Chemistry*. 2019; 1(2): 210-223.
[54] Nan J, Guo X, Xiao J, Li X, Chen W, Wu W, et al. Nanoengineering of 2D MXene-based materials for energy storage applications. *Small*. 2021; 17(9): 1902085.
[55] Kshetri T, Tran DT, Le HT, Nguyen DC, Van Hoa H, Kim NH, et al. Recent advances in MXene-based nanocomposites for electrochemical energy storage applications. *Progress in Materials Science*. 2021; 117: 100733.
[56] Xiong D, Li X, Bai Z, Lu S. Recent advances in layered $Ti_3C_2T_x$ MXene for electrochemical energy storage. *Small*. 2018; 14(17): 1703419.
[57] He S, Zhu Q, Soomro RA, Xu B. MXene derivatives for energy storage applications. *Sustainable Energy & Fuels*. 2020; 4(10): 4988-5004.
[58] Garg R, Agarwal A, Agarwal M. A review on MXene for energy storage application: Effect of interlayer distance. *Materials Research Express*. 2020; 7(2): 022001.
[59] Zhan C, Naguib M, Lukatskaya M, Kent PR, Gogotsi Y, Jiang DE. Understanding the MXene pseudocapacitance. *The Journal of Physical Chemistry Letters*. 2018; 9(6): 1223-1228.
[60] Luo J, Matios E, Wang H, Tao X, Li W. Interfacial structure design of MXene-based nanomaterials for electrochemical energy storage and conversion. *InfoMat*. 2020; 2(6): 1057-1076.
[61] Lee Y, Kim SJ, Kim YJ, Lim Y, Chae Y, Lee BJ, et al. Oxidation-resistant titanium carbide MXene films. *Journal of Materials Chemistry A*. 2020; 8(2): 573-581.
[62] Karataş Y, Çetin T, Akinay Y, Gülcan M. Synthesis and characterization of Pd doped MXene for hydrogen production from the hydrolysis of methylamine borane: Effect of cryogenic treatment. *Journal of the Energy Institute*. 2023; 109: 101310.
[63] Karataş Y, Çetin T, Akkuş İN, Akinay Y, Gülcan M. Rh(0) nanoparticles impregnated on two-dimensional transition metal carbides, MXene, as an effective nanocatalyst for ammonia-borane hydrolysis. *International Journal of Energy Research*. 2022; 46(8): 11411-11423.
[64] Ulas B, Çetin T, Kaya Ş, Akinay Y, Kivrak H. Novel $Ti_3C_2X_2$ MXene supported $BaMnO_3$ nanoparticles as hydrazine electrooxidation catalysts. *International Journal of Hydrogen Energy*. 2024; 58: 726-736.
[65] Jiang Q, Lei Y, Liang H, Xi K, Xia C, Alshareef HN. Review of MXene electrochemical microsupercapacitors. *Energy Storage Materials*. 2020; 27: 78-95.

[66] Alhabeb M, Maleski K, Anasori B, Lelyukh P, Clark L, Sin S, et al. Guidelines for synthesis and processing of two-dimensional titanium carbide ($Ti_3C_2T_x$ MXene). *Chemistry of Materials*. 2017; 29(18): 7633-7644.
[67] Shuck CE, Sarycheva A, Anayee M, Levitt A, Zhu Y, Uzun S, et al. Scalable synthesis of $Ti_3C_2T_x$ mxene. *Advanced Engineering Materials*. 2020; 22(3): 1901241.
[68] Ke CZ, Liu F, Zheng ZM, Zhang HH, Cai MT, Li M, et al. Boosting lithium storage performance of Si nanoparticles via thin carbon and nitrogen/phosphorus co-doped two-dimensional carbon sheet dual encapsulation. *Rare Metals*. 2021; 40(6): 1347-1356.
[69] Jawaid A, Hassan A, Neher G, Nepal D, Pachter R, Kennedy WJ, et al. Halogen etch of Ti_3AlC_2 MAX phase for MXene fabrication. *ACS Nano*. 2021; 15(2): 2771-2777.
[70] Lukatskaya MR, Halim J, Dyatkin B, Naguib M, Buranova YS, Barsoum MW, et al. Room-temperature carbide-derived carbon synthesis by electrochemical etching of MAX phases. *Angewandte Chemie*. 2014; 126(19): 4977-4980.
[71] Benchakar M, Loupias L, Garnero C, Bilyk T, Morais C, Canaff C, et al. One MAX phase, different MXenes: A guideline to understand the crucial role of etching conditions on $Ti_3C_2T_x$ surface chemistry. *Applied Surface Science*. 2020; 530: 147209.
[72] Li M, Lu J, Luo K, Li Y, Chang K, Chen K, et al. Element replacement approach by reaction with Lewis acidic molten salts to synthesize nanolaminated MAX phases and MXenes. *Journal of the American Chemical Society*. 2019; 141(11): 4730-4737.
[73] Persson I, El Ghazaly A, Tao Q, Halim J, Kota S, Darakchieva V, et al. Tailoring structure, composition, and energy storage properties of MXenes from selective etching of in-plane, chemically ordered MAX phases. *Small*. 2018; 14(17): 1703676.
[74] Kvashina TS, Uvarov NF, Korchagin MA, Krutskiy YL, Ukhina AV. Synthesis of MXene Ti_3C_2 by selective etching of MAX-phase Ti_3AlC_2. *Materials Today: Proceedings*. 2020; 31: 592-594.
[75] Sun W, Shah SA, Chen Y, Tan Z, Gao H, Habib T, et al. Electrochemical etching of Ti_2AlC to Ti_2CT_x (MXene) in low-concentration hydrochloric acid solution. *Journal of Materials Chemistry A*. 2017; 5(41): 21663-21668. Available from: https://doi.org/10.1039/C7TA05574A.
[76] Li T, Yao L, Liu Q, Gu J, Luo R, Li J, et al. Fluorine-free synthesis of high-purity $Ti_3C_2T_x$ (T = OH, O) via alkali treatment. *Angewandte Chemie International Edition*. 2018; 57(21): 6115-6119. Available from: https://doi.org/10.1002/anie.201800887.
[77] Song M, Pang SY, Guo F, Wong MC, Hao J. Fluoride-free 2D niobium carbide MXenes as stable and biocompatible nanoplatforms for electrochemical biosensors with ultrahigh sensitivity. *Advanced Science*. 2020; 7(24): 2001546.
[78] Zhang Q, He J, Fu X, Xie S, Fan R, Lai H, et al. Fluorine-free strategy for hydroxylated Ti_3C_2/Ti_3AlC_2 catalysts with enhanced aerobic oxidative desulfurization and mechanism. *Chemical Engineering Journal*. 2022; 430: 132950.
[79] Hu H, Bai Z, Niu B, Wu M, Hua T. Binder-free bonding of modularized MXene thin films into thick film electrodes for on-chip micro-supercapacitors with enhanced areal performance metrics. *Journal of Materials Chemistry A*. 2018; 6(30): 14876-14884.
[80] Ezika AC, Sadiku ER, Ray SS, Hamam Y, Folorunso O, Adekoya GJ. Emerging advancements in polypyrrole MXene hybrid nanoarchitectonics for capacitive energy storage applications. *Journal of Inorganic and Organometallic Polymers and Materials*. 2022; 32: 1-20. Available from: https://doi.org/10.1007/s10904-022-02280-6.
[81] Zhang YZ, El-Demellawi JK, Jiang Q, Ge G, Liang H, Lee K, et al. MXene hydrogels: Fundamentals and applications. *Chemical Society Reviews*. 2020; 49(20): 7229-7251.
[82] Bao Z, Lu C, Cao X, Zhang P, Yang L, Zhang H, et al. Role of MXene surface terminations in electrochemical energy storage: A review. *Chinese Chemical Letters*. 2021; 32(9): 2648-2658.
[83] Persson PO, Rosen J. Current state of the art on tailoring the MXene composition, structure, and surface chemistry. *Current Opinion in Solid State and Materials Science*. 2019; 23(6): 100774.
[84] Schultz T, Frey NC, Hantanasirisakul K, Park S, May SJ, Shenoy VB, et al.Surface termination dependent work function and electronic properties of $Ti_3C_2T_x$ MXene. *Chemistry of Materials*. 2019; 31(17): 6590-6597.
[85] Xia F, Lao J, Yu R, Sang X, Luo J, Li Y, et al. Ambient oxidation of Ti_3C_2 MXene initialized by atomic defects. *Nanoscale*. 2019; 11(48): 23330-23337.
[86] Habib T, Zhao X, Shah SA, Chen Y, Sun W, An H, et al. Oxidation stability of $Ti_3C_2T_x$ MXene nanosheets in solvents and composite films. *npj 2D Materials and Applications*. 2019; 3(1): 1-6.

[87] Chertopalov S, Mochalin VN. Environment-sensitive photoresponse of spontaneously partially oxidized Ti_3C_2 MXene thin films. *ACS Nano*. 2018; 12(6): 6109-6116.
[88] Yang S, Zhang P, Wang F, Ricciardulli AG, Lohe MR, Blom PWM, et al. Fluoride-free synthesis of two-dimensional titanium carbide (MXene) using a binary aqueous system. *Angewandte Chemie*. 2018; 130(47): 15717-15721. Available from: https://doi.org/10.1002/ange.201809662.
[89] Xuan J, Wang Z, Chen Y, Liang D, Cheng L, Yang X, et al. Organic-base-driven intercalation and delamination for the production of functionalized titanium carbide nanosheets with superior photothermal therapeutic performance. *Angewandte Chemie*. 2016; 128(47): 14789-14794.
[90] Wei Y, Zhang P, Soomro RA, Zhu Q, Xu B. Advances in the synthesis of 2D Mxenes. *Advanced Materials*. 2021; 33(39): 2103148.
[91] Yu L, Hu L, Anasori B, Liu YT, Zhu Q, Zhang P, et al. MXene-bonded activated carbon as a flexible electrode for high-performance supercapacitors. *ACS Energy Letters*. 2018; 3(7): 1597-1603.
[92] Fan Z, Wang D, Yuan Y, Wang Y, Cheng Z, Liu Y, et al. A lightweight and conductive MXene/graphene hybrid foam for superior electromagnetic interference shielding. *Chemical Engineering Journal*. 2020; 381: 122696.
[93] Bu F, Zagho MM, Ibrahim Y, Ma B, Elzatahry A, Zhao D. Porous MXenes: Synthesis, structures, and applications. *Nano Today*. 2020; 30: 100803.
[94] Wu X, Kang F, Duan W, Li J. Density functional theory calculations: a powerful tool to simulate and design high-performance energy storage and conversion materials. *Progress in Natural Science: Materials International*. 2019; 29(3): 247-255.
[95] Borysiuk VN, Mochalin VN, Gogotsi Y. Bending rigidity of two-dimensional titanium carbide (MXene) nanoribbons: A molecular dynamics study. *Computational Materials Science*. 2018; 143: 418-424.
[96] Borysiuk VN, Mochalin VN, Gogotsi Y. Molecular dynamic study of the mechanical properties of two-dimensional titanium carbides $Ti_{n+1}C_n$ (MXenes). *Nanotechnology*. 2015; 26(26): 265705. Available from: https://doi.org/10.1088/0957-4484/26/26/265705.
[97] Shuck CE, Han M, Maleski K, Hantanasirisakul K, Kim SJ, Choi J, et al. Effect of Ti_3AlC_2 MAX phase on structure and properties of resultant $Ti_3C_2T_x$ MXene. *ACS Applied Nano Materials*. 2019; 2(6): 3368-3376. Available from: https://doi.org/10.1021/acsanm.9b00286.
[98] Zhang C, Anasori B, Seral-Ascaso A, Park SH, McEvoy N, Shmeliov A, et al. Transparent, flexible, and conductive 2D titanium carbide (MXene) films with high volumetric capacitance. *Advanced Materials*. 2017; 29(36): 1702678.
[99] Sarycheva A, Gogotsi Y. Raman spectroscopy analysis of the structure and surface chemistry of $Ti_3C_2T_x$ MXene. *Chemistry of Materials*. 2020; 32(8): 3480-3488.
[100] Seredych M, Shuck CE, Pinto D, Alhabeb M, Precetti E, Deysher G, et al. High-temperature behavior and surface chemistry of carbide MXenes studied by thermal analysis. *Chemistry of Materials*. 2019; 31(9): 3324-3332.
[101] Guo M, Liu C, Zhang Z, Zhou J, Tang Y, Luo S. Flexible $Ti_3C_2T_x$@Al electrodes with ultrahigh areal capacitance: In situ regulation of interlayer conductivity and spacing. *Advanced Functional Materials*. 2018; 28(37): 1803196. Available from: https://doi.org/10.1002/adfm.201803196.
[102] Ando Y, Okubo M, Yamada A, Otani M. Capacitive versus pseudocapacitive storage in MXene. *Advanced Functional Materials*. 2020; 30(47): 2000820.
[103] Sun C, Wu C, Gu X, Wang C, Wang Q. Interface engineering via $Ti_3C_2T_x$ MXene electrolyte additive toward dendrite-free zinc deposition. *Nano-Micro Letters*. 2021; 13(1): 1-13.
[104] Kurra N, Uzun S, Valurouthu G, Gogotsi Y. Mapping (pseudo) capacitive charge storage dynamics in titanium carbide MXene electrodes in aqueous electrolytes using 3D bode analysis. *Energy Storage Materials*. 2021; 39: 347-353.
[105] Wang X, Fu Q, Wen J, Ma X, Zhu C, Zhang X, et al. 3D $Ti_3C_2T_x$ aerogels with enhanced surface area for high performance supercapacitors. *Nanoscale.* 2018; 10(44): 20828-20835.
[106] Naguib M, Mashtalir O, Lukatskaya MR, Dyatkin B, Zhang C, Presser V, et al. One-step synthesis of nanocrystalline transition metal oxides on thin sheets of disordered graphitic carbon by oxidation of MXenes. *Chemical Communications*. 2014; 50(56): 7420-7423.
[107] Tu S, Jiang Q, Zhang X, Alshareef HN. Large dielectric constant enhancement in MXene percolative polymer composites. *ACS Nano*. 2018; 12(4): 3369-3377.
[108] Gao L, Li C, Huang W, Mei S, Lin H, Ou Q, et al. MXene/polymer membranes: synthesis, properties, and emerging applications. *Chemistry of Materials*. 2020; 32(5): 1703-1747.
[109] Gong K, Zhou K, Qian X, Shi C, Yu B. MXene as emerging nanofillers for high-performance polymer composites: A review. *Composites Part B: Engineering*. 2021; 217: 108867.

[110]Ling Z, Ren CE, Zhao MQ, Yang J, Giammarco JM, Qiu J, et al. Flexible and conductive MXene films and nanocomposites with high capacitance. *Proceedings of the National Academy of Sciences*. 2014; 111(47): 16676-16681.
[111]Jimmy J, Kandasubramanian B. Mxene functionalized polymer composites: Synthesis and applications. *European Polymer Journal*. 2020; 122: 109367.
[112]Mayerberger EA, Urbanek O, McDaniel RM, Street RM, Barsoum MW, Schauer CL. Preparation and characterization of polymer-$Ti_3C_2T_x$ (MXene) composite nanofibers produced via electrospinning. *Journal of Applied Polymer Science*. 2017; 134(37): 45295.
[113]Kausar A. Polymer/MXene nanocomposite-a new age for advanced materials. *Polymer-Plastics Technology and Materials*. 2021; 60(13): 1377-1392.
[114]Hantanasirisakul K, Gogotsi Y. Electronic and optical properties of 2D transition metal carbides and nitrides (MXenes). *Advanced Materials*. 2018; 30(52): 1804779.
[115]Tripathi SN, Saini P, Gupta D, Choudhary V. Electrical and mechanical properties of PMMA/reduced graphene oxide nanocomposites prepared via in situ polymerization. *Journal of Materials Science*. 2013; 48(18): 6223-6232.
[116]Tasdelen MA, Van Camp W, Goethals E, Dubois P, Du Prez F, Yagci Y. Polytetrahydrofuran/clay nanocomposites by in situ polymerization and "click" chemistry processes. *Macromolecules*. 2008; 41(16): 6035-6040.
[117]Fim FD, Guterres JM, Basso NR, Galland GB. Polyethylene/graphite nanocomposites obtained by in situ polymerization. *Journal of Polymer Science Part A: Polymer Chemistry*. 2010; 48(3): 692-698.
[118]McDaniel RM, Carey MS, Wilson OR, Barsoum MW, Magenau AJ. Well-dispersed nanocomposites using covalently modified, multilayer, 2D titanium carbide (MXene) and in-situ "click" polymerization. *Chemistry of Materials*. 2021; 33(5): 1648-1656.
[119]Ul Haq Y, Murtaza I, Mazhar S, Ahmad N, Qarni AA, Ul Haq Z, et al. Investigation of improved dielectric and thermal properties of ternary nanocomposite PMMA/MXene/ZnO fabricated by in-situ bulk polymerization. *Journal of Applied Polymer Science*. 2020; 137(40): 49197.
[120]Wei S, Patil R, Sun L, Haldolaarachchige N, Chen X, Young DP, et al. Ex situ solvent-assisted preparation of magnetic poly (propylene) 8nocomposites filled with Fe@FeO nanoparticles. *Macromolecular Materials and Engineering*. 2011; 296(9): 850-857. Available from: https://doi.org/10.1002/mame.201100010.
[121]Zhang M, Yu A, Wu X, Shao P, Huang X, Ma D, et al. Sealing functional ionic liquids in conjugated microporous polymer membrane by solvent-assisted micropore tightening. *Nano Research*. 2022; 15(3): 2552-2557.
[122]Lu H, Zhang M, Yang Y, Huang Q, Fukuda T, Wang Z, et al. Solvent-assisted programming of flat polymer sheets into reconfigurable and self-healing 3D structures. *Nature Communications*. 2018; 9(1): 1-7.
[123]Altundağ A, Ünlü AE, Takaç S. Deep eutectic solvent-assisted synthesis of polyaniline by laccase enzyme. *Journal of Chemical Technology & Biotechnology*. 2021; 96(4): 1107-1115.
[124]Lin Y, Lu K, Davis R. Patterning of ZnO quantum dot and PMMA hybrids with a solvent-assisted technique. *Langmuir*. 2019; 35(17): 5855-5863.
[125]Simão C, Khunsin W, Kehagias N, Salaun M, Zelsmann M, Morris MA, et al. Order quantification of hexagonal periodic arrays fabricated by in situ solvent-assisted nanoimprint lithography of block copolymers. *Nanotechnology*. 2014; 25(17): 175703.
[126]Wang J, Song Y. Thin films and/or coating for electromagnetic interference and stealth. *Inorganic and Organic Thin Films: Fundamentals, Fabrication and Applications*. 2021; 2: 587-614.
[127]Jian X, He M, Chen L, Zhang M, Li R, Gao L, et al. Three-dimensional carambola-like MXene/polypyrrole composite produced by one-step co-electrodeposition method for electrochemical energy storage. *Electrochimica Acta*. 2019; 318: 820-827. Available from: https://doi.org/10.1016/j.electacta.2019.06.045.
[128]Elancheziyan M, Eswaran M, Shuck CE, Senthilkumar S, Elumalai S, Dhanusuraman R, et al. Facile synthesis of polyaniline/titanium carbide (MXene) nanosheets/palladium nanocomposite for efficient electrocatalytic oxidation of methanol for fuel cell application. *Fuel*. 2021; 303: 121329.
[129]Nasirpouri F, Alipour K, Daneshvar F, Sanaeian MR. Electrodeposition of anticorrosion nanocoatings. *Corrosion Protection at the Nanoscale*. Elsevier; 2020. p.473-497. Available from: https://doi.org/10.1016/B978-0-12-819359-4.00024-6.
[130]Li J, Levitt A, Kurra N, Juan K, Noriega N, Xiao X, et al. MXene-conducting polymer electrochromic microsupercapacitors. *Energy Storage Materials*. 2019; 20: 455-461.
[131]Popov A, Brasiunas B, Damaskaite A, Plikusiene I, Ramanavicius A, Ramanaviciene A. Electrodeposited gold nanostructures for the enhancement of electrochromic properties of PANI-PEDOT film deposited on transparent electrode. *Polymers*. 2020; 12(12): 2778.
[132]Popov A, Brasiunas B, Damaskaite A, Plikusiene I, Ramanavicius A, Ramanaviciene A. Doping of MXenes

enhances the electrochemical response of peptide-imprinted conductive polymers for the recognition of C-Reactive protein. *Biosensors and Bioelectronics*. 2022; 200: 113930.
[133]Feng Y, Zhou F, Dai Y, Xu Z, Deng Q, Peng C. High dielectric and breakdown performances achieved in PVDF/graphene@ MXene nanocomposites based on quantum confinement strategy. *Ceramics International*. 2020; 46(11): 17992-18001.
[134]Zhang Y, Choi JR, Park SJ. Thermal conductivity and thermo-physical properties of nanodiamond-attached exfoliated hexagonal boron nitride/epoxy nanocomposites for microelectronics. *Applied Science and Manufacturing*. 2017; 101: 227-236.
[135]Wang R, Zhuo D, Weng Z, Wu L, Cheng X, Zhou Y, et al. A novel nanosilica/graphene oxide hybrid and its flame retarding epoxy resin with simultaneously improved mechanical, thermal conductivity, and dielectric properties. *Journal of Materials Chemistry A*. 2015; 3(18): 9826-9836.
[136]Huang X, Zhi C, Lin Y, Bao H, Wu G, Jiang P, et al. Thermal conductivity of graphene-based polymer nanocomposites. *Materials Science and Engineering: R: Reports*. 2020; 142: 100577.
[137]Luo F, Wu K, Guo H, Zhao Q, Lu M. Simultaneous reduction and surface functionalization of graphene oxide for enhancing flame retardancy and thermal conductivity of mesogenic epoxy composites. *Polymer International*. 2017; 66(1): 98-107.
[138]Kang R, Zhang Z, Guo L, Cui J, Chen Y, Hou X, et al. Enhanced thermal conductivity of epoxy composites filled with 2D transition metal carbides (MXenes) with ultralow loading. *Scientific Reports*. 2019; 9(1): 9135.
[139]Zhang J, Kong N, Uzun S, Levitt A, Seyedin S, Lynch PA, et al. Scalable manufacturing of free-standing, strong $Ti_3C_2T_x$ MXene films with outstanding conductivity. *Advanced Materials*. 2020; 32(23): 2001093.
[140]Riazi H, Nemani SK, Grady MC, Anasori B, Soroush M. Ti_3C_2 MXene-polymer nanocomposites and their applications. *Journal of Materials Chemistry A*. 2021; 9(13): 8051-8098.
[141]Zha XH, Zhou J, Zhou Y, Huang Q, He J, Francisco JS, et al. Promising electron mobility and high thermal conductivity in Sc_2CT_2 (T = F, OH) MXenes. *Nanoscale*. 2016; 8(11): 6110-6117. Available from: https://doi.org/10.1039/C5NR08639F.
[142]Li L, Liu X, Wang J, Yang Y, Cao Y, Wang W. New application of MXene in polymer composites toward remarkable anti-dripping performance for flame retardancy. *Composites Part A: Applied Science and Manufacturing*. 2019; 127: 105649.
[143]Lee Y, Kim SJ, Kim YJ, Lim Y, Chae Y, Lee BJ, et al. Oxidation-resistant titanium carbide MXene films. *Journal of Materials Chemistry A*. 2020; 8(2): 573-581.
[144]Yao Y, Zeng X, Wang F, Sun R, Xu JB, Wong CP. Significant enhancement of thermal conductivity in bioinspired freestanding boron nitride papers filled with graphene oxide. *Chemistry of Materials*. 2016; 28(4): 1049-1057.
[145]Wang QW, Zhang HB, Liu J, Zhao S, Xie X, Liu L, et al. Multifunctional and water-resistant MXene-decorated polyester textiles with outstanding electromagnetic interference shielding and joule heating performances. *Advanced Functional Materials*. 2019; 29(7): 1806819.
[146]Jin X, Wang J, Dai L, Liu X, Li L, Yang Y, et al. Flame-retardant poly (vinyl alcohol)/MXene multilayered films with outstanding electromagnetic interference shielding and thermal conductive performances. *Chemical Engineering Journal*. 2020; 380: 122475.
[147]Cao Y, Deng Q, Liu Z, Shen D, Wang T, Huang Q, et al. Enhanced thermal properties of poly (vinylidene fluoride) composites with ultrathin nanosheets of MXene. *RSC Advances*. 2017; 7(33): 20494-20501.
[148]Ul Haq Y, Murtaza I, Mazhar S, Ahmad N, Qarni AA, Ul Haq Z, et al. Investigation of improved dielectric and thermal properties of ternary nanocomposite PMMA/MXene/ZnO fabricated by in-situ bulk polymerization. *Journal of Applied Polymer Science*. 2020; 137(40): 49197.
[149]Yan W, Zhang Y, Sun H, Liu S, Chi Z, Chen X, et al. Polyimide nanocomposites with boron nitride-coated multi-walled carbon nanotubes for enhanced thermal conductivity and electrical insulation. *Journal of Materials Chemistry A*. 2014; 2(48): 20958-20965.
[150]Wang F, Drzal LT, Qin Y, Huang Z. Mechanical properties and thermal conductivity of graphene nanoplatelet/epoxy composites. *Journal of Materials Science*. 2015; 50: 1082-1093.
[151]Kumar P, Yu S, Shahzad F, Hong SM, Kim YH, Koo CM. Ultrahigh electrically and thermally conductive self-aligned graphene/polymer composites using large-area reduced graphene oxides. *Carbon*. 2016; 101: 120-128.
[152]Gholivand H, Fuladi S, Hemmat Z, Salehi-Khojin A, Khalili-Araghi F. Effect of surface termination on the lattice thermal conductivity of monolayer $Ti_3C_2T_z$ MXenes. *Journal of Applied Physics*. 2019; 126(6): 065101. Available from: https://doi.org/10.1063/1.5094294.
[153]Mazhar S, Qarni AA, Haq YU, Haq ZU, Murtaza I. Promising PVC/MXene based flexible thin film nanocomposites with excellent dielectric, thermal and mechanical properties. *Ceramics International*. 2020; 46(8):

12593-12605.
[154]Liu R, Li W. High-thermal-stability and high-thermal-conductivity $Ti_3C_2T_x$ MXene/poly (vinyl alcohol) (PVA) composites. *ACS Omega*. 2018; 3(3): 2609-2617.
[155]Wang QW, Zhang HB, Liu J, Zhao S, Xie X, Liu L, et al. Multifunctional and water-resistant MXene-decorated polyester textiles with outstanding electromagnetic interference shielding and joule heating performances. *Advanced Functional Materials*. 2019; 29(7): 1806819.
[156]Wang J, Shen M, Liu Z, Wang W. MXene materials for advanced thermal management and thermal energy utilization. *Nano Energy*. 2022; 97: 107177.
[157]Faruk MO, Ahmed A, Jalil MA, Islam MT, Adak B, Hossain MM, et al. Functional textiles and composite based wearable thermal devices for Joule heating: progress and perspectives. *Applied Materials Today*. 2021; 23: 101025.
[158]Tabor J, Chatterjee K, Ghosh TK. Smart textile-based personal thermal comfort systems: Current status and potential solutions. *Advanced Materials Technologies*. 2020; 5(5): 1901155.
[159]Li L, Cao Y, Liu X, Wang J, Yang Y, Wang W. Multifunctional MXene-based fireproof electromagnetic shielding films with exceptional anisotropic heat dissipation capability and joule heating performance. *ACS Applied Materials & Interfaces*. 2020; 12(24): 27350-27360.
[160]Jiang L, Yuan L, Wang W, Zhang Q. Soft materials for wearable supercapacitors. *Soft Science*. 2021; 1: 5.
[161]Cui Y, Jiang Z, Zheng G, Wang W, Zhou M, Wang P, et al. Green preparation of PEDOT-based composites with outstanding electrothermal heating and durable rapid-response sensing performance for smart healthcare textiles. *Chemical Engineering Journal*. 2022; 446: 137189.
[162]Naguib M, Kurtoglu M, Presser V, Lu J, Niu J, Heon M, et al. Two-dimensional nanocrystals produced by exfoliation of Ti_3AlC_2. MXenes. *Jenny Stanford Publishing*. 2011; 23(37): 4248-4253. Available from: https://doi.org/10.1002/adma.201102306.
[163]Song P, Liu B, Qiu H, Shi X, Cao D, Gu J. MXenes for polymer matrix electromagnetic interference shielding composites: A review. *Composites Communications*. 2021; 24: 100653.
[164]Liu R, Miao M, Li Y, Zhang J, Cao S, Feng X. Ultrathin biomimetic polymeric $Ti_3C_2T_x$ MXene composite films for electromagnetic interference shielding. *ACS Applied Materials & Interfaces*. 2018; 10(51): 44787-44795.
[165]Wang Z, Cheng Z, Xie L, Hou X, Fang C. Flexible and lightweight $Ti_3C_2T_x$ MXene/Fe_3O_4@PANI composite films for high-performance electromagnetic interference shielding. *Ceramics International*. 2021; 47(4): 5747-5757.
[166]Zhang Y, Wang L, Zhang J, Song P, Xiao Z, Liang C, et al. Fabrication and investigation on the ultra-thin and flexible $Ti_3C_2T_x$/co-doped polyaniline electromagnetic interference shielding composite films. *Composites Science and Technology*. 2019; 183: 107833.
[167]Raagulan K, Braveenth R, Ro Lee L, Lee J, Kim BM, Moon JJ, et al. Fabrication of flexible, lightweight, magnetic mushroom gills and coral-like MXene-carbon nanotube nanocomposites for EMI shielding application. *Nanomaterials*. 2019; 9(4): 519.
[168]Raagulan K, Braveenth R, Kim BM, Lim KJ, Lee SB, Kim M, et al. An effective utilization of MXene and its effect on electromagnetic interference shielding: Flexible, free-standing and thermally conductive composite from MXene-PAT-poly(p-aminophenol)-polyaniline co-polymer. *RSC Advances*. 2020; 10(3): 1613-1633.
[169]Rajavel K, Luo S, Wan Y, Yu X, Hu Y, Zhu P, et al. 2D $Ti_3C_2T_x$ MXene/polyvinylidene fluoride (PVDF) nanocomposites for attenuation of electromagnetic radiation with excellent heat dissipation. *Composites Part A: Applied Science and Manufacturing*. 2020; 129: 105693.
[170]Zha XJ, Pu JH, Ma LF, Li T, Bao RY, Bai L, et al. A particular interfacial strategy in PVDF/OBC/MWCNT nanocomposites for high dielectric performance and electromagnetic interference shielding. *Composites Part A: Applied Science and Manufacturing*. 2018; 105: 118-125.
[171]Bhattacharjee Y, Chatterjee D, Bose S. Core-multishell heterostructure with excellent heat dissipation for electromagnetic interference shielding. *ACS Applied Materials & Interfaces*. 2018; 10(36): 30762-30773.
[172]Feng Y, Deng Q, Peng C, Hu J, Li Y, Wu Q, et al. An ultrahigh discharged energy density achieved in an inhomogeneous PVDF dielectric composite filled with 2D MXene nanosheets via interface engineering. *Journal of Materials Chemistry C*. 2018; 6(48): 13283-13292.
[173]Liang X, Garsuch A, Nazar LF. Sulfur cathodes based on conductive MXene nanosheets for high-performance lithium-sulfur batteries. *Angewandte Chemie*. 2015; 127(13): 3979-3983.
[174]Sobolčiak P, Ali A, Hassan MK, Helal MI, Tanvir A, Popelka A, et al. 2D $Ti_3C_2T_x$ (MXene)-reinforced polyvinyl alcohol (PVA) nanofibers with enhanced mechanical and electrical properties. *PLoS One*. 2017; 12(8): e0183705.
[175]Xu H, Yin X, Li X, Li M, Liang S, Zhang L, et al. Lightweight Ti_2CT_x MXene/poly (vinyl alcohol) composite foams for electromagnetic wave shielding with absorption-dominated feature. *ACS Applied Materials & Interfaces*.

2019; 11(10): 10198-10207.
[176]Sun R, Zhang HB, Liu J, Xie X, Yang R, Li Y, et al. Highly conductive transition metal carbide/carbonitride (MXene)@polystyrene nanocomposites fabricated by electrostatic assembly for highly efficient electromagnetic interference shielding. *Advanced Functional Materials*. 2017; 27(45): 1702807.
[177]Ling Z, Ren CE, Zhao MQ, Yang J, Giammarco JM, Qiu J, et al. Flexible and conductive MXene films and nanocomposites with high capacitance. *Proceedings of the National Academy of Sciences*. 2014; 111(47): 16676-16681.
[178]Liu F, Li Y, Hao S, Cheng Y, Zhan Y, Zhang C, et al. Well-aligned MXene/chitosan films with humidity response for high-performance electromagnetic interference shielding. *Carbohydrate Polymers*. 2020; 243: 116467.
[179]An H, Habib T, Shah S, Gao H, Radovic M, Green MJ, et al. Surface-agnostic highly stretchable and bendable conductive MXene multilayers. *Science Advances*. 2018; 4(3): 0118. Available from: https://doi.org/10.1126/sciadv.aaq0118.
[180]Wang L, Qiu H, Song P, Zhang Y, Lu Y, Liang C, et al. 3D $Ti_3C_2T_x$ MXene/C hybrid foam/epoxy nanocomposites with superior electromagnetic interference shielding performances and robust mechanical properties. *Composites Part A: Applied Science and Manufacturing*. 2019; 123: 293-300.
[181]Wang L, Chen L, Song P, Liang C, Lu Y, Qiu H, et al. Fabrication on the annealed $Ti_3C_2T_x$ MXene/Epoxy nanocomposites for electromagnetic interference shielding application. *Composites Part B: Engineering*. 2019; 171: 111-118.
[182]Song P, Qiu H, Wang L, Liu X, Zhang Y, Zhang J, et al. Honeycomb structural rGO-MXene/epoxy nanocomposites for superior electromagnetic interference shielding performance. *Sustainable Materials and Technologies*. 2020; 24: e00153.
[183]Liu J, Zhang HB, Sun R, Liu Y, Liu Z, Zhou A, et al. Hydrophobic, flexible, and lightweight MXene foams for high-performance electromagnetic-interference shielding. *Advanced Materials*. 2017; 29(38): 1702367.
[184]Liu Y, Zhang J, Zhang X, Li Y, Wang J. $Ti_3C_2T_x$ filler effect on the proton conduction property of polymer electrolyte membrane. *ACS Applied Materials & Interfaces*. 2016; 8(31): 20352-20363.
[185]Luo JQ, Zhao S, Zhang HB, Deng Z, Li L, Yu ZZ. Flexible, stretchable and electrically conductive MXene/natural rubber nanocomposite films for efficient electromagnetic interference shielding. *Composites Science and Technology*. 2019; 182: 107754.
[186]Mayerberger EA, Urbanek O, McDaniel RM, Street RM, Barsoum MW, Schauer CL. Preparation and characterization of polymer-$Ti_3C_2T_x$ (MXene) composite nanofibers produced via electrospinning. *Journal of Applied Polymer Science*. 2017; 134(37): 45295.
[187]Naguib M, Saito T, Lai S, Rager MS, Aytug T, Paranthaman MP, et al. $Ti_3C_2T_x$ (MXene)-polyacrylamide nanocomposite films. *RSC Advances*. 2016; 6(76): 72069-72073.
[188]Tanvir A, Sobolčiak P, Popelka A, Mrlik M, Spitalsky Z, Micusik M, et al. Electrically conductive, transparent polymeric nanocomposites modified by 2D $Ti_3C_2T_x$ (MXene). *Polymers*. 2019; 11(8): 1272.
[189]Zhan Z, Song Q, Zhou Z, Lu C. Ultrastrong and conductive MXene/cellulose nanofiber films enhanced by hierarchical nano-architecture and interfacial interaction for flexible electromagnetic interference shielding. *Journal of Materials Chemistry C*. 2019; 7(32): 9820-9829.
[190]Cao WT, Chen FF, Zhu YJ, Zhang YG, Jiang YY, Ma MG, et al. Binary strengthening and toughening of MXene/cellulose nanofiber composite paper with nacre-inspired structure and superior electromagnetic interference shielding properties. *ACS Nano*. 2018; 12(5): 4583-4593.
[191]Zhao J, Liu F, Li W. Phosphate ion-modified RuO_2/Ti_3C_2 composite as a high-performance supercapacitor material. *Nanomaterials*. 2019; 9(3): 377.
[192]Idumah CI, Ezeani OE, Okonkwo UC, Nwuzor IC, Odera SR. Novel trends in MXene/conducting polymeric hybrid nanoclusters. *Journal of Cluster Science*. 2023; 34(1): 45-76.
[193]Dong Y, Guan S, Zhou X, Chang Q, Jiang G. Co-intercalation of CTAB favors the preparation of $Ti_3C_2T_x$/PANI composite with improved electrochemical performance. *Ionics*. 2021; 27: 2501-2508.
[194]Dong K, Yang Z, Chen J, Shi D, Chen M. Oxygen vacancy-Fe_2O_3@polyaniline composites directly grown on carbon cloth as a high stable electrode for symmetric supercapacitors. *Journal of Inorganic and Organometallic Polymers and Materials*. 2021; 31(9): 3894-3903.
[195]Fu J, Yun J, Wu S, Li L, Yu L, Kim KH. Architecturally robust graphene-encapsulated MXene Ti_2CT_x@Polyaniline composite for high-performance pouch-type asymmetric supercapacitor. *ACS Applied Materials & Interfaces*. 2018; 10(40): 34212-34221.
[196]Wu W, Wang C, Zhao C, Wei D, Zhu J, Xu Y. Facile strategy of hollow polyaniline nanotubes supported on Ti_3C_2-

MXene nanosheets for high-performance symmetric supercapacitors. *Journal of Colloid and Interface Science*. 2020; 580: 601-613.
[197]Yun J, Echols I, Flouda P, Wang S, Easley A, Zhao X, et al. Layer-by-layer assembly of polyaniline nanofibers and MXene thin-film electrodes for electrochemical energy storage. *ACS Applied Materials & Interfaces*. 2019; 11(51): 47929-47938.
[198]Zhou W, Kuang W, Liang X, Zhou W, Guo J, Gan L, et al. Exploration of MXene/polyaniline composites as promising anode materials for sodium ion batteries. *Journal of Physics D: Applied Physics*. 2020; 54(6): 064001.
[199]Li Y, Kamdem P, Jin XJ. Hierarchical architecture of MXene/PANI hybrid electrode for advanced asymmetric supercapacitors. *Journal of Alloys and Compounds*. 2021; 850: 156608.
[200]Wang S, Ma Z, Lü QF, Yang H. Two-dimensional $Ti_3C_2T_x$/polyaniline nanocomposite from the decoration of small-sized graphene nanosheets: promoted pseudocapacitive electrode performance for supercapacitors. *ChemElectroChem*. 2019; 6(10): 2748-2754.
[201]Zou Y, Zhang Z, Zhong W, Yang W. Hydrothermal direct synthesis of polyaniline, graphene/polyaniline and N-doped graphene/polyaniline hydrogels for high performance flexible supercapacitors. *Journal of Materials Chemistry A*. 2018; 6(19): 9245-9256.
[202]Boota M, Anasori B, Voigt C, Zhao MQ, Barsoum MW, Gogotsi Y. Pseudocapacitive electrodes produced by oxidant-free polymerization of pyrrole between the layers of 2D titanium carbide (MXene). *Advanced Materials*. 2016; 28(7): 1517-1522. Available from: https://doi.org/10.1002/adma.201504705.
[203]Zhang X, Wang J, Liu J, Wu J, Chen H, Bi H. Design and preparation of a ternary composite of graphene oxide/carbon dots/polypyrrole for supercapacitor application: Importance and unique role of carbon dots. *Carbon*. 2017; 115: 134-146.
[204]Zhu J, Xu Y. Enhanced electrochemical performance of polypyrrole depending on morphology and structure optimization by reduced graphene oxide as support frameworks. *Electrochimica Acta*. 2018; 265: 47-55.
[205]Liang W, Zhitomirsky I. MXene-polypyrrole electrodes for asymmetric supercapacitors. *Electrochimica Acta*. 2022; 406: 139843.
[206]Wei D, Wu W, Zhu J, Wang C, Zhao C, Wang L. A facile strategy of polypyrrole nanospheres grown on Ti_3C_2-MXene nanosheets as advanced supercapacitor electrodes. *Journal of Electroanalytical Chemistry*. 2020; 877: 114538.
[207]Wu W, Wei D, Zhu J, Niu D, Wang F, Wang L, et al. Enhanced electrochemical performances of organ-like Ti_3C_2 MXenes/polypyrrole composites as supercapacitors electrode materials. *Ceramics International*. 2019; 45(6): 7328-7337.
[208]Mahajan M, Singla G, Ogale S. Polypyrrole-encapsulated polyoxomolybdate decorated MXene as a functional 2D/3D nanohybrid for a robust and high performance Li-ion battery. *ACS Applied Energy Materials*. 2021; 4(5): 4541-4550.
[209]Yan J, Ma Y, Zhang C, Li X, Liu W, Yao X, et al. Polypyrrole-MXene coated textile-based flexible energy storage device. *RSC Advances*. 2018; 8(69): 39742-39748.
[210]Wustoni S, Saleh A, El-Demellawi JK, Koklu A, Hama A, Druet V, et al. MXene improves the stability and electrochemical performance of electropolymerized PEDOT films. *APL Materials*. 2020; 8(12): 121105. Available from: https://doi.org/10.1063/5.0023187.
[211]Hwang SK, Patil SJ, Chodankar NR, Huh YS, Han YK. An aqueous high-performance hybrid supercapacitor with MXene and polyoxometalates electrodes. *Chemical Engineering Journal*. 2022; 427: 131854.
[212]Wang X, Sun K, Li K, Li X, Gogotsi Y. $Ti_3C_2T_x$/PEDOT: PSS hybrid materials for room-temperature methanol sensor. *Chinese Chemical Letters*. 2020; 31(4): 1018-1021.
[213]Tseghai GB, Mengistie DA, Malengier B, Fante KA, Van Langenhove L. PEDOT: PSS-based conductive textiles and their applications. *Sensors*. 2020; 20(7): 1881.
[214]Zhang M, Heraly F, Yi M, Yuan J. Multitasking tartaric-acid-enabled, highly conductive, and stable MXene/conducting polymer composite for ultrafast supercapacitor. *Cell Reports Physical Science*. 2021; 2(6): 100449. Available from: https://doi.org/10.1016/j.xcrp.2021.100449.
[215]Li L, Zhang N, Zhang M, Zhang X, Zhang Z. Flexible $Ti_3C_2T_x$/PEDOT: PSS films with outstanding volumetric capacitance for asymmetric supercapacitors. *Dalton Transactions*. 2019; 48(5): 1747-1756.
[216]Qin L, Tao Q, El Ghazaly A, Fernandez-Rodriguez J, Persson PO, Rosen J, et al. High-performance ultrathin flexible solid-state supercapacitors based on solution processable Mo1. 33C MXene and PEDOT: PSS. *Advanced Functional Materials*. 2018; 28(2): 1703808.
[217]Li J, Jin Q, Yin F, Zhu C, Zhang X, Zhang Z. Effect of $Ti_3C_2T_x$-PEDOT: PSS modified-separators on the

electrochemical performance of Li-S batteries. *RSC Advances*. 2020; 10(66): 40276-40283.
[218]Bai S, Guo X, Chen T, Zhang Y, Zhang X, Yang H, et al. Solution processed fabrication of silver nanowire-MXene@PEDOT: PSS flexible transparent electrodes for flexible organic light-emitting diodes. *Composites Part A: Applied Science and Manufacturing*. 2020; 139: 106088. Available from: https://doi.org/10.1016/j.compositesa.2020.106088.
[219]VahidMohammadi A, Moncada J, Chen H, Kayali E, Orangi J, Carrero CA, et al. Thick and freestanding MXene/PANI pseudocapacitive electrodes with ultrahigh specific capacitance. *Journal of Materials Chemistry A*. 2018; 6(44): 22123-22133.